Technical Note N-1314

A FLUIDIC SYSTEM FOR MIXING TWO FLUIDS -- FINAL STUDY

by

D. Pal

December 1973

Sponsored by

DIRECTOR OF NAVY LABORATORIES

NAVAL CIVIL ENGINEERING LABORATORY
Port Hueneme, California 93043

A FLUIDIC SYSTEM FOR MIXING TWO FLUIDS - FINAL STUDY

Technical Note N-1314

ZFXX-512-001-005

by

D. Pal

ABSTRACT

The development of a double leg elbow proportional fluid amplifier to handle 5.85 gpm of water flow rate is described in detail. The amplifier has linear output flow characteristics with a gain of 50 and can switch flow from one output to the other completely. Based upon the experimental results, analytical expressions are developed which clearly show the effects of the active and passive legs flow parameters, the control flow, and the size and location of the output ports on amplifier's performance and they can be used in designing an amplifier of a desired flow capacity. Analytical expressions to predict the performance of the amplifier are also given. A mixing element comprised of two double leg elbow amplifiers stacked together to mix two fluids was designed and tested successfully.

CONTENTS

INTRODUCTION

A study conducted at the Naval Civil Engineering Laboratory (NCEL) showed that mixing of two or more fluids in desired proportions is feasible by using proportional fluid amplifiers.[1] The operational principle of such mixing systems is based upon the flow modulating characteristics, an unique feature, of most proportional fluid amplifiers. A proposed concept of a fluidic system[2] suitable for mixing two fluids is shown in Figure 1. The system uses two double leg elbow proportional amplifiers, one for each fluid. The fluid amplifiers control the flow of two fluids to mix them in the desired ratios. The amplifiers are controlled by the signals tapped off from the venturi orifice on the mixture line. For changing the mixture ratio a variable fluid resistor is provided on the control line of each fluid amplifier. These variable resistors are fluidic passive devices consisting of a resistance path either of a variable length or of a variable cross-section which is varied with a control knob.

Due to some definite advantages[1] offered by the fluidic components, a research program was initiated to develop a fluidic system for mixing hot and cold water capable of handling 5 gpm of each fluid. During this program it was found necessary to develop a double leg elbow amplifier with a 0-5 gpm output flow range since this component is not available commercially. Following successful development of a suitable amplifier, a mixing system was designed and was tested by mixing water from two sources. The report describes in detail the entire development program of the mixing system.

DOUBLE LEG ELBOW AMPLIFIER

Consider the amplifier shown in Figure 2, in which the flow through its active leg, in the form of a short radius elbow, is interacted by a small flow through its control port. Further, the flow through the passive leg of the amplifier combines with that through the active leg at its exit and forms a jet which is called the "power jet" in the Fluid State terminlogy. The emanating angle of the power jet can be changed either by regulating the supply flow or by varying the flow through the control port. However, the efflux velocity of the power jet can be changed by varying the supply flow only. The proportional deflection of the power jet by the control flow can then be utilized in dividing the supply flow between the two output ports of the amplifier to obtain a proportional action. Development of such an amplifier to handle 5 gpm of water is described in the following sections of the report.

Table 1. Parameters of the Designed Experimental Element.

Amplifiers parameters	Designed values (before the tests)	Modified values (after the tests)
1. <u>Active Leg</u>		
Width, w_a	5/8 inch	1/2 inch
Depth, h	1/2 inch	1/2 inch
Inner wall radius, r_i	1/2 inch	1/2 inch
Outer wall radius, r_o	1-1/4 inch	1 inch
Cross-sectional area, A_a	0.3125 $inch^2$	0.2500 $inch^2$
Hydraulic diameter, d_a	0.5556 inch	0.5000 inch
Designed flow, Q_a	2.5 gpm	Table 4
Reynolds number* at the designed flow, $\frac{U_a d_a}{\nu}$	9,903	Table 4
2. <u>Passive Leg</u>		
Width, w_p	3/8 inch	3/8 inch
Depth, h	1/2 inch	1/2 inch
Cross-sectional area, A_p	0.1875 $inch^2$	0.1875 $inch^2$
Hydraulic diameter, d_p	0.4286 inch	0.4286 inch
Designed flow, Q_p	2.5 gpm	Table 4
Reynolds number* at the designed flow, $\frac{U_p d_p}{\nu}$	12,732	Table 4
Angle between the active and the passive legs	90°	90°

Table 1. Parameters of the Designed Experimental Element. (Continued)

Amplifiers parameters	Designed values (before the tests)	Modified values (after the tests)
3. <u>Control Port</u>		
Width, w_c	1/16 inch	1/32 inch
Depth, h	1/2 inch	1/2 inch
Cross-sectional area, A_c	0.03125 $inch^2$	0.01563 $inch^2$
Location	Figure 4	Figure 7
Type of control	Injection	Injection
4. <u>Power Jet Separation Surface</u>	Figure 5	Figure 7

* Kinematic viscosity (ν) of water at $60^{o}F$ was taken as 1.2×10^{-5} ft^2/sec.

AMPLIFIER DEVELOPMENT

A double leg elbow amplifier was designed and built to determine its performance. After a series of laboratory tests, each followed by some modifications in the amplifier's parameters, the amplifier did perform as a proportional device.[2] However, some problems existed in that the amplifier delivered a fluctuating flow; and also its output versus input characteristics were not as linear as desired. Therefore, efforts were devoted towards developing a suitable amplifier for use in the mixing system.

Experimental Element Design

The important considerations in the design of a double leg elbow amplifier are the proper design of the active and passive leg flow passages, location and size of the control port, and the shape of the power jet separation surface. The flow pattern through the amplifier is complex and cannot be realized by the existing theory. Some experimental work has been reported on flow characteristics in rectangular curved passages. Practically all of this work is based upon fully developed inlet velocity profiles and most of the researchers experimented with large radii channels only.[3,4] None of these publications report curved channel flows with injection into or suction from the separation region of the channel. However, the work of Curtiss, Feil and Liquornik[5], primarily experimental in nature, deals with studies on curved channel flows with injection into its separation region. The reported work using some empirical assumptions describes flows in curved channels of varying curvatures with relatively small bend radii. The results of this study were utilized by Curtiss and Liquornik[6] in developing a double leg elbow amplifier operating on air. The amplifier was used for signal amplification only. The work described in reference 5, although very exhaustive, does not develop any general criteria for the location of the control port and for the proper design of the power jet separation surface (Figure 2). Furthermore, the authors did not study the effect of passive leg flow on the active leg flow and hence on the power jet deflection. It was therefore felt that, to develop the desired amplifier a systematic experimental study be undertaken to determine the following:

1. Suitable dimensions of the active and passive legs.

2. For the selected active and passive leg dimensions, determine by trial and error the size and configuration of the control port and the shape of the power jet separation surface.

3. Finally, obtain the control flow versus power jet deflection characteristics for the experimental element. These characteristics were used in designing the location and size of the amplifier's output ports, and in developing a theory for predicting its performance.

Thus an experimental element was designed and built. Based upon the results of reference 5, the active leg was designed with an aspect ratio (depth/width) of 0.8 and ratio of its radii (inner radius/outer radius) as 0.20 such that the separation in the bend will occur naturally. From the momentum balance considerations one can see that the angle between the active and the passive legs of the element can be anywhere from 0 to 180°. However, the 90° angle makes the power jet emanating angle very sensitive to the passive leg flow without decreasing its axial momentum appreciably. The dimensions of the active and passive leg flow passages were determined for a designed flow of 2.5 gpm each. The corresponding flow Reynolds number through the supply flow passages was in the range of 13,000. A sketch of the element is shown in Figure 3. The control for the element was of counter flow type secondary injection. The control slot was extended the full depth of the channel with a width of 1/16 inches. The location and other pertinent details of the control slot are shown in Figure 4. The details of the power jet separation surface of the element are shown in Figure 5. Further, Table 1 lists the dimensions and important parameters of the designed element.

Experimental Program

A test program was designed to determine the suitable design of the element by trial and error procedure. Extensive tests were run to derive the element's characteristics.

The experiments were conducted in the Mechanical Systems Laboratory at NCEL using regular tap water as the working fluid under carefully controlled flow and pressure conditions. All experiments were performed under continuous flow conditions so that sufficient time was available for stabilization of all flows and instrument readings. The general arrangement of various flow lines and instruments of the test setup are shown in the schematic of Figure 6. The adjustment of the supply flow is possible by the hand controlled valves provided on the line. The control flow to the element was provided by means of a pumping system capable of creating positive pressure in the line. The element remained immersed in water throughout the test series.

Supply and control flows were measured by rotameters. Static pressures were measured by the conventional pressure gages. Throughout the test program, a dye injection technique was used for flow visualization through the element. This method consisted of injecting a concentrated solution of methyl blue (a blue dye) through the ports

Table 2. Various Flow Rates through the Element for Each Test Series.

Test Series	Flow through the		Flow through control port (gpm) for observation no.					
	Active leg (gpm)	Passive leg (gpm)	1	2	3	4	5	6
1	4.0	3.50	0	0.015	0.030	0.045	0.60	0.105
2	3.0	3.0	0	0.020	0.040	0.060	0.080	0.120
3	4.5	3.5	0	0.0130	0.025	0.038	0.051	---
4	5.0	4.0	0	0.012	0.024	0.036	0.048	---

located on the right and left sides of the power jet through the cover plates by means of a dye injection pump system. Due to submerged nature of the power jet the dye solution was trapped by the entrained flow thereby making the flow pattern in the element visible. The technique was very successful in revealing the power jet boundaries. Photographs of the flow pattern were taken by mounting a camera directly above the element.

Test Results

Some modifications in the location of the control port and in the shape of the power jet separation surface resulted from the tests. The width of the active leg flow passage was reduced to ½ inch. All modifications that were necessary for the proper functioning of the element are shown in a sketch (Figure 7). Table 1 lists the dimensions of the various parameters of the element after modifications. The flow through the active and passive leg of the modified element changed which resulted in new flow Reynolds numbers (22000 range). A typical flow pattern through the element for flow rates of 4.0 gpm and 3.5 gpm through its active and passive legs respectively with no control flow is shown in Figure 8.

Power Jet Deflection Characteristics

Tests to obtain jet versus control flow characteristics were conducted on the modified element. Altogether four series of tests, with different combinations of active and passive leg flows (Table 2) were run. For each series the control flow was varied discretely from zero to some value which deflected the power jet by 20°. For each observation a photograph of the flow pattern through the element was taken for record and analysis. Out of a total of 26 pictures taken, 12 are included in the report for illustration (Figures 8 through 19). During the experiments it was observed and is apparent from the flow pattern photographs that the flow through the element was highly turbulent. It was further noticed that the maximum sensitivity of the power jet occurred at flow rates of 5.0 gpm and 4.0 gpm through the active and passive legs respectively.

Further, the power jet deflection was measured from the flow pattern photographs for each test series. In addition to this the power jet width was measured at distances of three and four inches from the interaction zone of the supply flows. Table 3 lists the power jet deflection and its width for the entire test series. Furthermore, to determine the trend in the experimental data, the jet deflection, $\Delta\Psi$, was plotted against Q_c/Q_a for each Q_p/Q_a (Figure 20). Where Q_p, Q_a, and Q_c are the flow rates through the passive and active legs, and through the control port of the element respectively. It should be noted from Figure 20 that these characteristics are nearly straight lines and the maximum sensitivity of the power jet occurs for

Table 3. Power Jet Deflection Data.

Active and Passive leg flow combinations	Control flow, Q_c (gpm)	$\frac{Q_c}{Q_a}$	Power jet angle (degrees)	Power jet deflection (degrees) $\Delta\psi$	Power jet width in inches at	
					3 inches	4 inches
Q_a = 3.0 gpm;	0	0	21.5 (ψo)	0	0.85	1.00
Q_p = 3.0 gpm	0.06	0.02	24.0	2.5	0.90	1.10
	0.12	0.04	26.5	5.0	0.80	1.05
	0.18	0.06	29.5	8.0	0.80	1.10
	0.24	0.08	32.5	11.0	0.80	1.10
	0.36	0.12	37.5	16.0	0.80	1.10
Q_a = 4.0 gpm;	0	0	25.0 (ψo)	0	1.05	1.35
Q_p = 3.5 gpm	0.06	0.015	28.0	3.0	1.15	1.40
	0.12	0.030	31.0	6.0	1.05	1.35
	0.18	0.045	34.0	9.0	1.15	1.30
	0.24	0.060	37.0	12.0	1.10	1.35
	0.42	0.105	45.5	20.5	1.10	1.35

(Continued)

Table 3. Power Jet Deflection Data. (Continued)

Active and Passive leg flow combinations	Control flow, Q_c (gpm)	$\frac{Q_c}{Q_a}$	Power jet angle (degrees)	Power jet deflection (degrees) $\Delta\psi$	Power jet width in inches at	
					3 inches	4 inches
Q_a = 4.5 gpm;	0	0	33.0 (ψo)	0	1.30	1.50
Q_p = 3.5 gpm	0.06	0.013	37.0	4.0	1.25	1.50
	0.12	0.025	42.0	9.0	1.25	1.50
	0.18	0.038	47.0	14.0	1.25	1.50
	0.24	0.051	51.0	18.0	1.25	1.50
Q_a = 5.0 gpm;	0	0	29.0 (ψo)	0	1.0	1.25
Q_p = 4.0 gpm	0.060	0.012	34.5	5.5	1.0	1.30
	0.12	0.024	39.5	10.5	1.1	1.25
	0.18	0.036	44.5	15.5	1.1	1.25
	0.24	0.048	49.5	20.5	1.1	1.30

$Q_p = 4.0$ gpm and $Q_a = 5.0$ gpm.

For a given power jet separation surface, the slopes of its deflection characteristics depend upon the active and passive leg flow passage dimensions, and the flows through them. Thus, if it is the slope of the power jet characteristics, then

$$s = s\ (Q_a,\ Q_p,\ h,\ w_a,\ w_p)\ Q_c/Q_a, \tag{1}$$

or

$$s = s\ (Q_a,\ Q_p/Q_a,\ h,\ w_a,\ w_a,\ w_p)\ Q_c/Q_a. \tag{2}$$

where h = depth of the flow passages

w_a = width of the active leg

and w_p = width of the passive leg

Hence, from Figure 20, the power jet deflection, $\Delta\psi$, using Equation (2) can be written as

$$\Delta\psi = s(Q_a,\ Q_p,\ Q_a,\ h,\ w_a,\ w_a/w_p)\ Q_c/Q_a\ , \tag{3-a}$$

or simply

$$\Delta\psi = Q_c/Q_a. \tag{3-b}$$

In Equation (3-b), if $\Delta\psi$ is expressed in degrees, then the units of s are in degrees. Further, s for each characteristic curve can be calculated using Equation (3-b). Table 4 shows values of s for various Q_a, Q_p/Q_a for the element with fixed h, w_a and w_a/w_p.

Amplifier Theory

The interacting active and passive flows of the element shown in Figure 21, combine to form the power jet. If M_a and M_p are the momentum of the active and passive leg flows respectively, then the momentum of the power jet, M_r. is given by

$$M_r = \sqrt{M_a^{\ 2} + M_p^{\ 2}}\ . \tag{4}$$

Equation (4) holds for the configuration shown in Figure 21 only where the angle between the active and passive legs is 90°. Further, the momentum of the active and passive leg flows in terms of their flow rates and flow passage area, neglecting static pressure changes are given as

Table 4. Power Jet Characteristics Slope Data.

Flow passages depth, h	= 0.5000 inches
Active leg passage width, w_a	= 0.5000 inches
Hydraulic diameter of the active leg passage, d_a	= 0.5000 inches
Passive leg passage width, w_p	= 0.3750 inches
Hydraulic diameter of the passive leg passage, d_p	= 0.4286 inches
Ratio, w_a/w_p	= 1.333 inches

Active leg flow, Q_a (gpm)	3.0	4.0	4.5	5.0
Active leg flow Reynolds number, $\frac{U_a d_a}{\nu}$	13,368	17,824	20,052	22,280
Passive leg flow, Q_p (gpm)	3.0	3.5	3.5	4.0
Passive leg flow Reynolds number, $\frac{U_p d_p}{\nu}$	15,279	17,825	17,825	20,372
Ratio, Q_p/Q_a	1.00	0.875	0.778	0.800
Slope, s (degrees)	133.33	195.24	352.94	427.08

$$M_a = \frac{\rho Q_a^2}{w_a h} \quad , \qquad (5\text{-}a)$$

and
$$M_p = \frac{\rho Q_p^2}{w_p h} \quad . \qquad (5\text{-}b)$$

where ρ is the mass density of the fluid. Thus from Equations (4), (5-a) and (5-b) after simplification, one obtains

$$M_r = \frac{\rho Q_a^2}{w_a h} \sqrt{1 + \left(\frac{w_a}{w_p}\right)^2 \left(\frac{Q_p}{Q_a}\right)^4} \quad . \qquad (6)$$

Again, the power jet after it leaves the separation surface, behaves like a turbulent two dimensional jet. Analytical expressions for the velocity distribution of such jets are derived in Schlichting[7] and the expression for the axial component of the jet velocity is given below

$$u(x,y) = U(x) \ \mathrm{Sech}^2 \left(\frac{\sigma y}{x}\right) \quad . \qquad (7)$$

where $u(x,y)$ = axial component of velocity,

$U(x)$ = center line velocity,

= 7.67, a free constant.

Figure 22 illustrates the jet co-ordinate system and its axial velocity profile for $\sigma = 7.67$. It is obvious from the jet axial velocity profile that the slope of the jet spread i.e., angle α (Figure 22) is

$$\alpha = \tan^{-1} (0.3) = 16.7^{\circ} \quad . \qquad (8)$$

The value of α calculated in Equation (8) is based upon the value of y where the axial velocity drops to four percent of the center line velocity, i.e., where $\frac{u(x,y)}{U(x)} = 0.04$. Based upon this, the width of the jet is given by the equation

$$2b(x) = 0.60\ x + 2b_o \tag{9}$$

where 2b(x) is the width of the jet (Figure 22) and $2b_o$ is the nozzle width. Now, the momentum, M_j, of the jet, which is constant along the jet is given by

$$M_j = \frac{4}{3}\,\rho\, U^2(x)\ \frac{xh}{\sigma} \tag{10}$$

Since the axial momentum of the jet remains constant along x, thus M_r expressed in Equation (6), which relates the power jet momentum M_r to the momenta of active and passive leg flows, must be equal to M_j, i.e., ($M_j = M_r$). Hence, from Equations (6) and (10) the following expressions results

$$\frac{U(x)\ h\sqrt{xw_a}}{Q_a} = \sqrt{\frac{3}{4}\ \ \sigma\sqrt{1 + \left(\frac{w_a}{w_p}\right)^2 \left(\frac{Q_p}{Q_a}\right)^4}} \tag{11-a}$$

By defining

$$\frac{U(x)\ \ h\sqrt{xw_a}}{Q_a} = \beta \tag{11-b}$$

Equation (11-a) can be reduce to

$$\beta = \sqrt{\frac{3}{4}\ \ \sigma\sqrt{1 + \left(\frac{w}{w_p}\right)^2 \ \ \left(\frac{Q_p}{Q_a}\right)^4}} \tag{11-c}$$

with the active and passive leg flow parameters. A solution of Equation (11-c) is shown in a plot of Figure 23, where the dimensionless parameter $\frac{U(x)\ \ h\sqrt{xw_a}}{Q_a} = \beta$ is plotted against $\frac{w_a}{w_p}\left(\frac{Q_p}{Q_a}\right)^2$.

This result is used in locating the output ports of the amplifier.

Finally the power jet flows into the output ports in proportion to the deflection of the jet. Proper location and size of the output flow passages is very important. Now a procedure for designing the output ports of the amplifier will be given. A general layout of the output port geometry is shown in Figure 24. Notice that points A, B

Table 5. Output Port Width for Various Combinations of the Active and Passive Leg Flows.

Active leg flow, Q_a (gpm)	3.0	4.0	4.5	5.0
Passive leg flow, Q_p (gpm)	3.0	3.5	3.5	4.0
Output port width w_o, for x_o = 3 inches	0.838	1.07	0.942	1.07
Output port width, w_o for x_o = 4 inches	1.12	1.43	1.260	1.43

and C are arranged such that when the power jet deflects, the x co-ordinate of each point is x_o. The output ports layout is such that the power jet axis coincides with that of the Port O_L. Thus angle of the port O_L axis is equal to φ_o as shown in Figure 24. Further, the width, w_o, of each port is derived from Equation (3-b) as

$$w_o = x_o \frac{s}{57.3} \left(\frac{Q_c}{Q_a} \right)_{max} , \quad (12)$$

where $\left(\frac{Q_c}{Q_a} \right)_{max}$ = maximum dimensionless control flow corresponding to the maximum deflection, $\Delta\psi_{max}$, of the power jet.

57.3 = a factor for converting degrees into radians

x_o = co-ordinate of the splitter tip

As an illustration Table 5 give the values of output port, w_o, for x_o = 3 and 4 inches respectively for various combinations of the active and passive legs Q_a and Q_p. The angular location of the output port is achieved on the basis of the power jet emanating angle with no control flow, i.e., ψ_o . This angle for various combinations of the active and passive leg flows was measured and recorded in Table 3. Further, the co-ordinates of points A, B, and C change with the control flow and can be obtained using Equation (12). These are given below:

$$x_a = x_o , \quad (13\text{-a})$$

$$y_a = - \frac{x_o \; s}{2 \times 57.3} \left[\left(\frac{Q_c}{Q_a} \right)_{max} + 2 \left(\frac{Q_c}{Q_a} \right) \right] , \quad (13\text{-b})$$

$$x_b = x_o , \quad (13\text{-c})$$

$$y_b = \frac{x_o \; s}{2 \times 57.3} \left[\left(\frac{Q_c}{Q_a} \right)_{max} - 2 \left(\frac{Q_c}{Q_a} \right) \right] , \text{ and} \quad (13\text{-d})$$

$$x_c = x_o . \quad (13\text{-e})$$

$$y_c = \frac{x_o \ s}{2 \times 57.3} \left[3\left(\frac{Q_c}{Q_a}\right)_{max} - 2\left(\frac{Q_c}{Q_a}\right) \right] . \qquad (13\text{-f})$$

The location of output ports of the amplifier can be assigned using Equations (13-a) through (13-f) for zero power jet deflection. Thus the co-ordinates of the points A, B, and C (Figure 24) for zero control flow are:

$$x_{ao} = x_o \quad , \qquad (14\text{-a})$$

$$y_{ao} = \frac{x_o \ s}{2 \times 57.3} \left(\frac{Q_c}{Q_a}\right)_{max} = \frac{x_o s \ (Q_c / Q_a)_{max}}{114.6} \quad , \qquad (14\text{-b})$$

$$x_{bo} = x_o \quad , \qquad (14\text{-c})$$

$$y_{bo} = \frac{xos}{2 \times 57.3} \left(\frac{Q_c}{Q_a}\right)_{max} = \frac{x_o \ s \ (Q_c / Q_a)_{max}}{114.6} \quad , \qquad (14\text{-d})$$

$$x_{co} = x_o \quad , \qquad (14\text{-e})$$

$$y_{co} = \frac{3 \ x \ s}{2 \times 57.3} \left(\frac{Q_c}{Q_a}\right)_{max} = \frac{3x_o s \ (Q_c / Q_a)_{max}}{114.6} \quad . \qquad (14\text{-f})$$

Since point A is fixed, points B and A can be fixed using Equations (14-a) through (14-f). The included angle, δ , of the splitter is such (about 3^o) that the ports form a smooth flow passage.

Flow Through The Output Ports

After designing proper output ports, the next logical step is to deduce the output flow characteristics of the amplifier. The flow through the output ports can be analytically determined for a given position of the jet using relationships shown in Figure 24. Knowing the power jet velocity from Equation (7) and the jet configuration from Figure 24, the flow Q_{OL} through the output port O_L is

$$Q_{OL} = \int_{y_a}^{y_b} h\, U(x_o)\, \mathrm{Sech}^2\left(\frac{\sigma y}{x_o}\right) dy \qquad (15)$$

and the flow Q_{OR} through the output port O_R is

$$Q_{OR} = \int_{y_b}^{y_c} h\, U(x_o)\, \mathrm{Sech}^2\left(\frac{\sigma y}{x_o}\right) dy \qquad (16)$$

Further by integrating Equations (15) and (16) and using Equations (13-a) through (13-f) for value of y_a, y_b, and y_c, one obtains

$$Q_{OL} = \frac{U(x_o)\, x_o h}{\sigma} \left[\tanh \frac{\sigma s}{114.6} \left[(Q_c/Q_a)_{max} - 2(Q_c/Q_a) \right] + \tanh \frac{\sigma s}{114.6} \left[(Q_c/Q_a)_{max} + 2(Q_c/Q_a) \right] \right] \qquad (17)$$

and

$$Q_{OR} = \frac{U(x_o)\, x_o h}{\sigma} \left[\tanh \frac{\sigma s}{114.6} \left[3\,(Q_c/Q_a)_{max} - 2(Q_c/Q_a) \right] - \tanh \frac{\sigma s}{114.6} \left[(Q_c/Q_a)_{max} - 2\,(Q_c/Q_a) \right] \right] . \qquad (18)$$

Further, recall from Equation (11-b) that

$$\beta = \frac{U(x)h\sqrt{x w_a}}{Q_a} = \frac{U(x_o)h\sqrt{x_o\, w_a}}{Q_a} \qquad (19)$$

Table 6. Computed Values of Parameter $\frac{Q_o}{Q_a} \frac{\sigma}{\beta} \sqrt{\frac{w_a}{x_o}}$ as a function of Q_c/Q_a

S. No.	Power Jet Parameters	Dimension less control flow	$\frac{Q_{OR}}{Q_a} \frac{\sigma}{\beta} \sqrt{\frac{w_a}{x_o}}$	$\frac{Q_{OL}}{P_a} \frac{\sigma}{\beta} \sqrt{\frac{w_a}{x_o}}$
1	Active leg flow, Q_{OR} = 3.0 gpm	0	0.2072	1.579
		0.02	0.3804	1.504
	Passive leg flow, Q_{OL} = 3.0 gpm	0.04	0.6446	1.287
		0.06	0.9727	0.9727
	s = 133.33	0.08	1.287	0.6446
		0.12	1.579	0.2072
2	Active leg flow, Q_a = 4.0 gpm	0	0.1208	1.878
		0.015	0.2460	1.696
	Passive leg flow, Q_p = 3.5 gpm	0.030	0.4690	1.502
	s = 195.24	0.045	0.8014	1.186
		0.060	1.180	0.8060
		0.105	1.878	0.1208
3	Active leg flow, Q_a = 4.5 gpm	0	0.1648	1.767
		0.013	0.4651	1.479
	Passive leg flow, Q_p = 3.5 gpm	0.025	0.9577	1.009
	s = 352.94	0.038	1.478	0.4651
		0.051	1.767	0.1648
4	Active leg flow, Q_a = 5.0 gpm	0	0.1208	1.757
		0.012	0.4040	1.558
	Passive leg flow, Q_p = 4.0 gpm	0.024	0.9790	0.9790
	s = 427.08	0.036	1.559	0.4040
		0.048	1.757	0.1208

Therefore, by substituting for $U(x_o)$, Equations (17) and (18) can be rewritten as

$$\frac{Q_{OL}}{Q_a}\frac{\sigma}{\beta}\sqrt{\frac{w_a}{x_o}} = \left[\tanh\frac{\sigma s}{114.6}\left[(Q_c/Q_a)_{max} - 2(Q_c/Q_a)\right] + \tanh\frac{\sigma s}{114.6}\left[(Q_c/Q_a)_{max} + 2(Q_c/Q_a)\right]\right] \quad (20)$$

and

$$\frac{Q_{OR}}{Q_a}\frac{\sigma}{\beta}\sqrt{\frac{w_a}{x_o}} = \left[\tanh\frac{\sigma s}{114.6}\left[3(Q_c/Q_a)_{max} - 2(Q_c/Q_a)\right] - \tanh\frac{\sigma s}{114.6}\left[(Q_c/Q_a)_{max} - 2(Q_c/Q_a)\right]\right] \quad (21)$$

It should be noted here that β which appears in Equations (20) and (21) is a function of the passive to active legs flow ratio and of the ratio of the widths of the active to passive legs flow passages. Thus, the output flow described by the above equations is a function of the active and passive leg flows, the active and passive leg flow passages geometric parameters, the power jet deflection characteristics slope, the distance of the splitter from the supply flow interation point and the dimensionless control flow. Solutions of these equations are obtained for the active and passive leg flows combinations shown in Table 4. These solutions are listed in Table 6 and are shown in Figure 25, in which parameters $\frac{Q_{OR}}{Q_a}\frac{\sigma}{\beta}\sqrt{\frac{w_a}{x_o}}$ and $\frac{Q_{OL}}{Q_a}\frac{\sigma}{\beta}\sqrt{\frac{w_a}{x_o}}$ are plotted against the dimensionless control flow Q_c/Q_a. It should be noted from Figure 25 and from Equations (20) and (21) that the output flow can be switched completely from one port to the other. Thus, ideally for the maximum deflection of the power jet, that about 90 percent

Table 7. Geometric Parameters of the Designed Double Leg Elbow Fluid Amplifier.

1. Active Leg	
Width, w_a	1/2 inch
Depth, h	3/8 inch
Inner wall radius, r_i	1/2 inch
Outer wall radius, r_o	1 inch
Cross-sectional area, A_a	0.125 $inch^2$
2. Passive Leg	
Width, w_p	1/4 inch
Depth, h	3/8 inch
Cross-sectional area, A_p	0.0625 $inch^2$
Angle between active and passive legs	90^o
3. Control Port	
Width, w_c	1/32 inch
Depth, h	3/8 inch
Cross-sectional area, A_c	0.0078 $inch^2$
Location	See Figure 26
Type of control	Injection
4. Output Port	
Width, w_o	1 inch
Depth, h	3/8 inch
Number of ports	2
Cross-sectional area, A_o	0.250 $inch^2$
Splitter location, x_o	3-1/4 inches from the point of interaction of the active and passive leg flows

flow of the total can be switched proportionately from one output port to the other. However, in an actual amplifier this is not true because corresponding to 10 percent of the total flow the flow velocity through the output port is so small that its velocity head is not enough to cause any flow.

THE PROTOTYPE AMPLIFIER

Design of the Amplifier

Based upon the theory developed in the previous section, a double leg elbow amplifier was designed to handle 5 gpm of water flow rate. The geometric parameters of the active and passive legs, the control port and the power jet separation of the amplifier were kept the same as that of the experimental element (Table 1). However, the depth h, of the flow passages was reduced to 3/8-inch to increase the power jet momentum for a given combination of active and passive leg flows. It was assumed that the designed values of Q_a and Q_p were 2.5 gpm each such that

$$\frac{w_a}{w_p}\left(\frac{Q_p}{Q_a}\right)^2 = 2.0,$$

resulting in a value of 3.59 for the parameter

$$\beta = \frac{U(x_o)\ h\sqrt{x_o w_a}}{Q_a} .$$

It was further assumed that to force the flow through the output ports, the stagnation pressure of the power jet based upon its axial velocity $U(x_o)$, i.e., $\frac{U^2(x_o)}{2g}$ should not be less than three inches corresponding to $U(x_o)$ of four ft/sec. Using this data, x_o was found to be 5.6 inches. Due to other practical considerations, however, x_o was chosen to be 3.25 inches. The maximum deflection of the power jet was assumed to be 18°. Further, using Equation (12) the width w_o of the output ports for $x_o = 3.25$, was computed as one inch. For this configuration of the output ports, $U(x_o)$ was calculated by using the value of β and was found to be four ft/sec. Table 7 lists the values of all the key geometric parameters of the amplifier. The vents were provided on either side of the power jet to prevent wall attachment effects. The vents were designed such that they can be connected to the output ports, if desired. A sketch of the amplifier's element is shown in Figure 26.

Table 8. Test data taken at the optimum performance of the amplifier.

Supply pressure, P_s	= 12.0 psig
Active leg flow, Q_a	= 2.30 gpm
Passive leg flow, Q_p	= 3.55 gpm
The ratio, Q_p/Q_a	= 1.54
The parameter, $\frac{w_a}{w_p}\left(\frac{Q_p}{Q_a}\right)^2$	= 4.74
Maximum deflection of the power jet, $\Delta\psi$	= 22^{o}
Slope of the power jet characteristics, s	= 188
Corresponding value of the parameter, β (From Equa. 11c)	= 5.30
Geometric parameter, $\frac{w_a}{x_o}$ of the amplifier	= 0.308
Therefore, $\frac{\sigma}{\beta}\sqrt{\frac{w_a}{x_o}}$	= 0.805

No.	Control Port Flow		Flow through the Port O_L		Flow through the Port O_R	
	Q_c gpm	Q_c/Q_a	Q_{OL} gpm	Q_{OL}/Q_a	Q_{OR} gpm	Q_{OR}/Q_a
1	0.0	0.0	5.85	2.05	0.0	0.0
2	0.033	0.014	5.00	1.75	0.853	0.300
3	0.067	0.029	4.09	1.43	1.70	0.595
4	0.100	0.043	3.40	1.19	2.57	0.90
5	0.133	0.058	2.54	0.89	3.46	1.21
6.	0.200	0.087	1.05	0.368	5.00	1.75
7	0.267	0.116	0.0	0.0	6.10	2.13

The amplifier consists of three major components: top and bottom cover plates, and the middle plate, called the amplifier's elements, with the flow passages machined in it. The middle plate is made of aluminum and the flow passages in it were machined by milling process. The top cover plate is made of transparent plexi-glass sheet to facilitate flow visualization during tests, whereas, the bottom cover plate is a 1/4-inch thick aluminum sheet. Before assembling the amplifier, the two surfaces of its element were coated with a thin layer of silicon grease to ensure a leak proof assembly. The assembled amplifier, with the pipe fittings for connecting hoses ready for testing is shown in Figure 27.

Tests and Performance Characteristics

Testing of the amplifier was necessary to determine its performance. The tests were conducted using the test setup shown in Figure 6. A photograph of the setup showing the amplifier undergoing tests is shown in Figure 28. For a combination of active and passive leg flows, the control flow was varied stepwise from zero to some optimum value and back to zero. Since the amplifier is a low impedance device, the flow through its output ports can not be measured by high impedance devices such as rotamaters and orifices. Thus, the flow through the output ports was measured with a calibrated bucket and a stop watch. It is worth mentioning here that for the proper operation of the amplifier, the vent on the left of its power jet was connected to the output O_L whereas the one on its right side was connected to the output O_R . This arrangement prevented occurrence of low pressure regions inside the amplifier caused by the power jet deflection.

After a series of tests, the operating parameters for the optimum performance of the amplifier were determined and are listed in Table 8. It can be seen from the test data that the active and passive leg flows at the optimum operating point are 2.30 and 3.55 gpm respectively. Correspondingly the flow through the output ports varies from 5.85 to zero gpm in the port O_R and from zero to 6.10 gpm in the port O_L when the control flow is changed from zero to 0.267 gpm. Photographs of the flow patterns in the amplifier were taken; two of these taken at zero and 0.267 gpm control flow respectively are shown in Figure 29 and 30. It is evident from the records that the flow patterns consisted of a strong vortex on the left side of the power jet. Because of turbulent nature of the flow through the amplifier about three percent flow fluctuation $\left(\frac{Q_{o_{max}} - Q_{o_{min}}}{Q_{o\ mean}}\right)$ was observed. The output flow verses control flow characteristics for the amplifier were plotted from the test data and are shown in Figure 31. The flow characteristics are linear over about 80 percent of the operating control flow range. It should be noted further that the flow amplification factor (defined as $\Delta Q_o / \Delta Q_c$) for the amplifier is about 50, which is considerably higher compared to the other fluid state proportional devices[8] with a corresponding maximum value of 10. Further, it can be seen from the test data (Table 8) that the maximum control flow for operating the amplifier is about 4.6 percent of the total supply flows. These features make the amplifier suitable for applications where sensitivity and low control flows are required. Another attractive quality of the amplifier is that it can switch flow from one output port to the other completely. Thus the amplifier is a suitable metering device for mixing systems. To make an evaluation of the amplifier's performance and to verify the theory developed earlier its dimensionless output flow characteristics were obtained in the manner described here. From the known Q_p and Q_a at a given operation condition, the parameter

$\frac{w_a}{w_p}\left(\frac{Q_p}{Q_a}\right)^2$ is computed. Further, by recalling that for a known value of $\frac{w_a}{w_p}$ parameter β can be obtained either from Equation (11-c) or directly from the curve shown in Figure 23. Since x_o, w_a, and σ are known, dimensionless output flow parameter $\frac{Q_o}{Q_a}\frac{\sigma}{\beta}\sqrt{\frac{w_a}{x_o}}$ is calculated for each value through the output ports, O_L, and O_R. The data on the dimensionless characteristics thus computed are listed in Table 8, whereas a plot of $\frac{Q_c}{Q_a}\frac{\sigma}{\beta}\sqrt{\frac{w_a}{x_o}}$ verses $\frac{Q_c}{Q_a}$ is shown in Figure 32. Further, theoretical values of output flow $\frac{Q_o}{Q_a}\frac{\sigma}{\beta}\sqrt{\frac{w_a}{x_o}}$ for various Q_c/Q_a were calculated from Equations (20) and (21). Value of s, required in the above calculations was obtained from the consideration that the power jet deflects by 22^o while the control flow changes from zero to 0.267 gpm. The theoretical characteristics are plotted on the same plot as the experimental characteristics (Figure 32) for comparison. It can be seen from Figure 32 that the experimental values of the parameter $\frac{Q_o}{Q_a}\frac{\sigma}{\beta}\sqrt{\frac{w_a}{x_o}}$ differ from its theoretical values by as much as 10 percent.

The deviation of the experimental values from the theoretical values is attributed primarily to the effect of the output port impedance on the power jet and the magnitude of the control flow, not added to power jet flow. It is evident, however, that the experimental characteristics are linear over a wide range of the control flow and the output flow can be switched completely from one port to the other. It is therefore concluded that the amplifier can be designed using the theoretical procedure described in the report, but its output flow characteristics should be derived experimentally.

In summary, it can be stated that as desired a double leg elbow amplifier capable of delivering about five gpm of water flow rate has been developed. The amplifier has a flow amplification factor of 50 and is capable of switching flow completely from one output to the other proportionately. The output flow characteristics of the amplifier are nearly linear. Finally, a theory to predict the output flow and useful in designing an amplifier of given capability has been developed. The theory predicts amplifiers outflow within 10 percent of its actual value.

THE FLUIDIC MIXING SYSTEM

The mixing system shown in Figure 1 employs amplifiers that operate on suction type controls only. But the proportional amplifier developed here required a blowing type control thus the concept needs modification. Therefore the design of a system must be modified accordingly. One such system design is shown in Figure 33 in which two modulating amplifiers are manually controlled by connecting the control port of each amplifier to a source of fluid source through variable resistors to vary the flow. A given mixture flow at a certain mixture ratio is obtained simply by adjusting the control flow for each amplifier. Similarly, the mixture ratio at a certain mixture flow rate can be varied simply by adjusting the needle valves settings. Fluidic variable resistors such as variable length, variable area, or variable curvature type for a given application can be fabricated. However, their resistance can not be varied uniformly from zero to no flow. Mechanically operated needle valves suffer from maintenance problems, however, their resistance characteristics are such that they can modulate flows from a predetermined value to zero. Such valves can be fabricated from corrosion resistant materials to reduce frequent maintenance. These valves because of their low flow carrying capacity (up to 0.2 gpm) are small and cost of replacing them is much lower than those of capacities up to 5 gpm. In the light of the foregoing discussion it was decided to use needle valves on the control lines of the mixing system. Such a mixing system is free from water hammer problems (in case of liquids) because there is no sudden closure of valves during operation. Furthermore, becasue of sensitive amplifiers, the system has a fast response. Consequently, it was decided to test the system by mixing water with water.

Table 9. Mixing System Test Data.

Amplifier s_1
Active leg flow - 2.32 gpm
Passive leg flow - 3.55 gpm

Amplifier s_2
Active leg flow - 2.30 gpm
Passive leg flow - 3.54 gpm

Test Series No.	Amplifier s_1		Amplifier s_2 Control flow from Q_{C2} (gpm) Flow are the output Port 02 and mixture ratio $m_2 = Q_{02}/Q_{01}$									
			0.025		0.050		0.100		0.200		0.250	
	Control Flow Qcl gpm	Output Flow 001	Q_{02}	m_2	Q_{02}	m_2	Q_{02}	m_2	Q_{02}	m_2	Q_{02}	m_2
1	0.033	5.00	5.22	1.044	4.60	0.92	3.40	0.68	1.05	0.21	0.20	0.04
2	0.100	3.42	5.25	1.535	4.65	1.36	3.40	0.994	1.02	0.298	0.20	0.058
3	0.133	2.55	5.15	2.02	4.62	1.812	3.35	1.314	1.02	0.40	0.22	0.086
4	0.200	1.05	5.20	4.95	4.62	4.4	3.35	3.19	1.05	1.0	0.22	0.2095

Mixing Element and the Test Results

The two amplifiers of the system were combined to form one single element for compatness. The element in this configuration consists of one amplifier mounted on top of the other. The amplifiers are separated by 1/4-inch thick aluminum plate; the top and bottom cover plates of the mixing element are 3/4-inch thick plexi-glass plates for visualization. The disassembled parts of the element are shown in Figure 34 and the assembled element ready to undergo tests is shown in Figure 35.

The mixing element was tested on the test setup as shown schematically in Figure 36 and photographically in Figure 37. Mixing tests were conducted under several configurations by running fresh water through each amplifier circuit. Corresponding to a fixed setting of control on one amplifier, the control on the other was varied discretely from zero to the designed value of 0.267 gpm. Since the amplifier operates on a very low output impedance, the flow through the drain side output line of each amplifier was measured using a calibrated bucket and a stop watch. The flow through the mixing side output line of each amplifier was computed by subtracting the flow through the drainside output line from the sum of the supply and the control flows. The reduced data from mixing tests is shown in Table 9. As can be seen by examining Table 9, the system performed well, i.e., each amplifier operated as predicted. The interaction of the mixing side output flows of the amplifier did not affect the operation of the amplifier.

DISCUSSION

It is interesting to note that the system can be automated as shown by the concept of Figure 38. According to this design the control flow to each modulating amplifier is supplied by a controlling amplifier of the proportional type. The supply flow to each controlling amplifier can be varied by a needle valve provided on its line. The control port of each amplifier is connected to the mixing line side output of the moderating amplifier. The change of pressure in the lines 01M and 02M (Figure 38) due to change in mixture demand is communicated to the controlling amplifier which in turn sends a required signal flow into the control port of each modulating amplifier to deliver some definite flow. The controlling amplifier circuitory can be designed such that for no mixture demand the controlling amplifiers do not send any signal to the modulating amplifiers. The valves on the controlling amplifiers can be calibrated such that the mixture ratio of the fluids being mixed can be changed simply by varying their settings. Such a system in addition to having fast response is free from hybrid sensors which utilize electrical signals.

Further, an amplifier capable of modulating gas flows can be designed using the technique described in the report. Therefore, a system to mix gases can be designed. One restraint on such a system is that the flow through the amplifiers must be incompressible which means the supply pressures should be in the 2 psig range.

CONCLUSIONS

1. A double leg elbow amplifier capable of modulating water flow rate of 5.85 gpm with linear output flow characteristics was developed. The amplifier has a relatively high gain of 50 and can modulate the flow through its output from 5.85 gpm to zero when the control flow is changed from zero to 0.267 gpm. Because of low pressure inside the amplifier, it is extremely sensitive to the output impedance and thus its output ports must be designed carefully for its proper operation.

2. Analytical expressions which predict the amplifiers output flow within 10 percent of their actual values were developed. These expressions are also useful in designing a double leg elbow, amplifier with a given flow capacity.

3. A mixing system using two such amplifiers was designed and tested successfully by mixing a liquid with a liquid. A system to mix gases can be designed by the method and the theory discussed in the report.

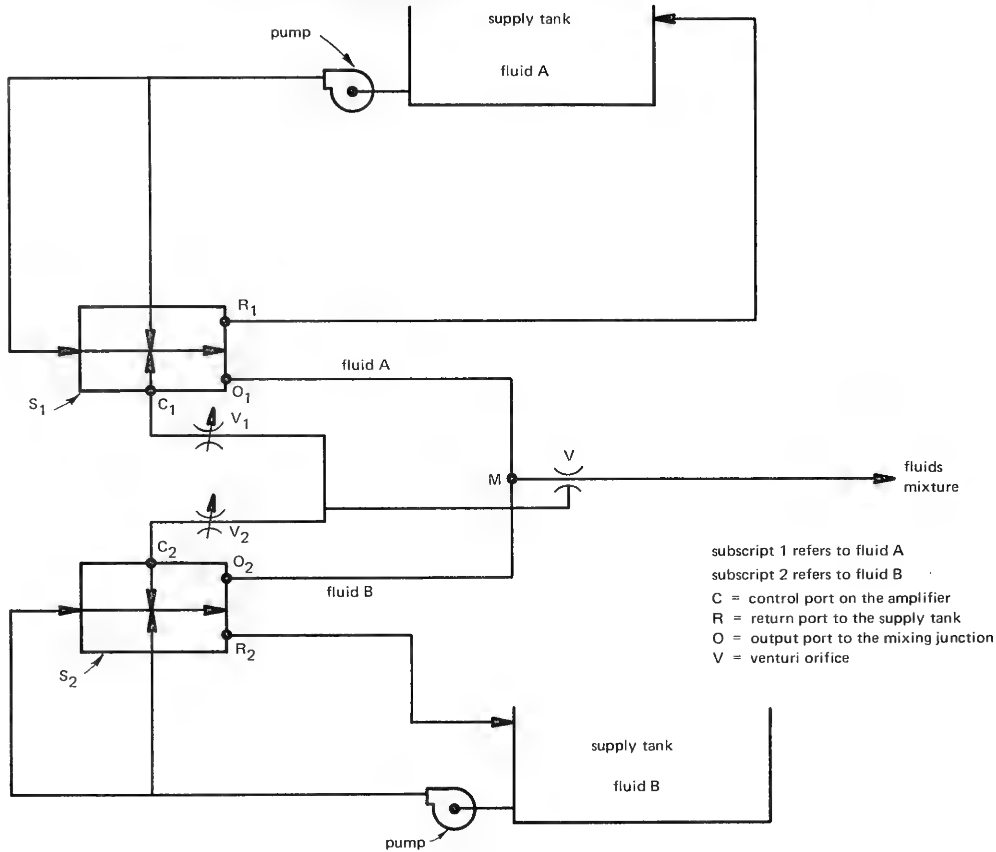

Figure 1. A fluidic system for mixing two fluids.

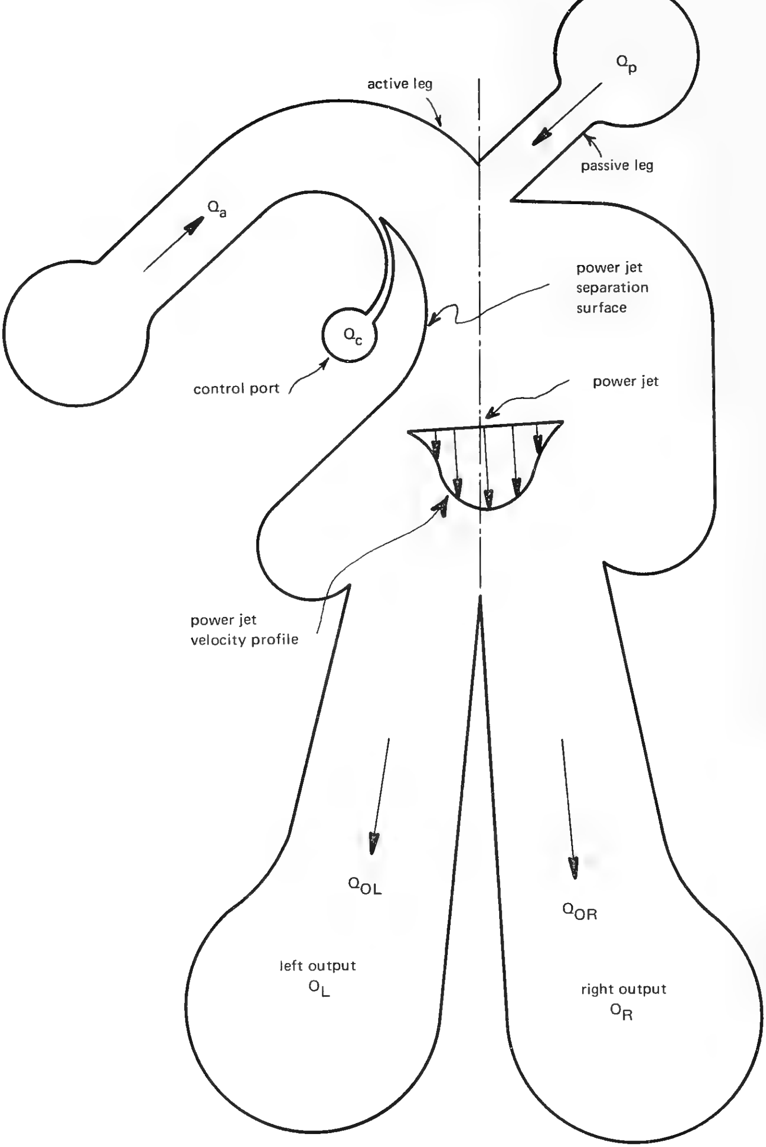

Figure 2. Double leg elbow amplifier sketch.

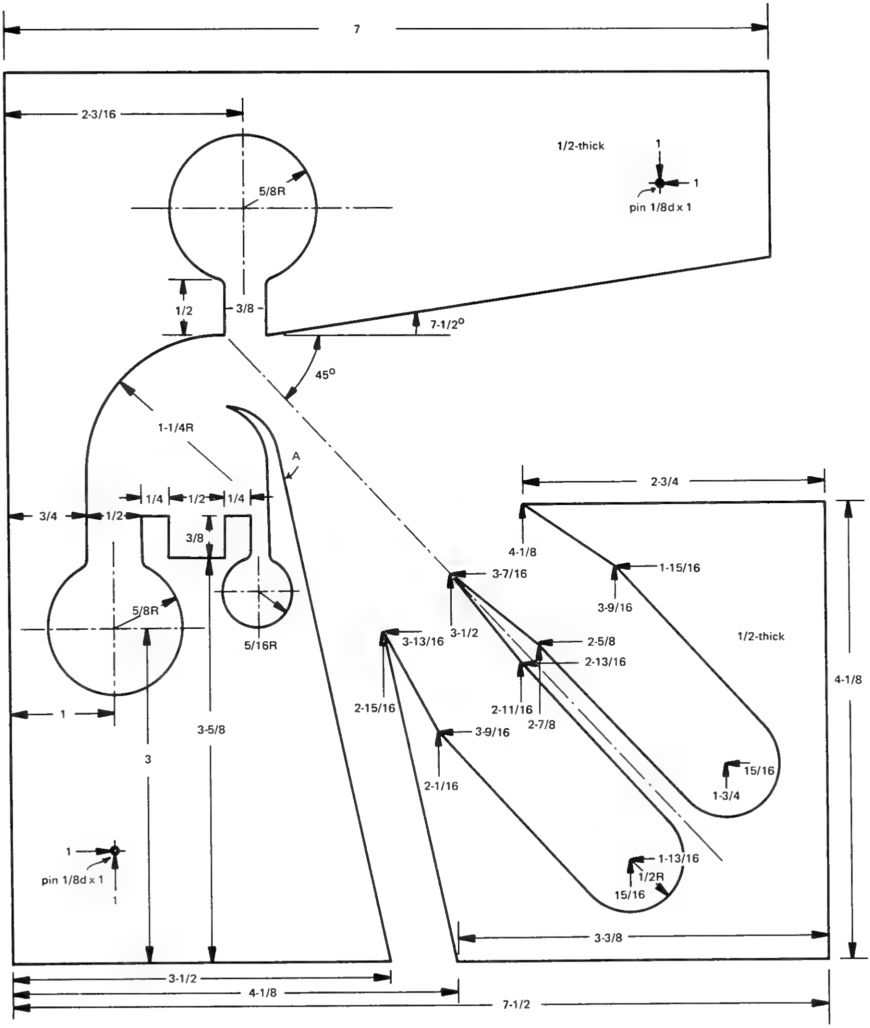

Figure 3. Sketch of the experimental amplifier.

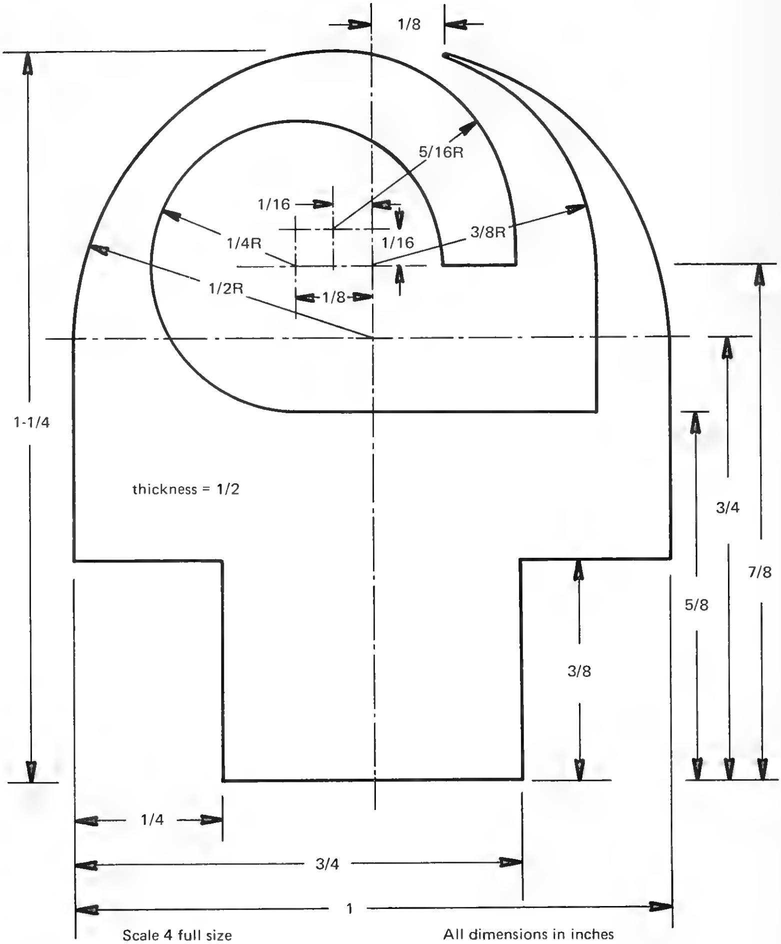

Figure 4. Details of control port on the designed element.

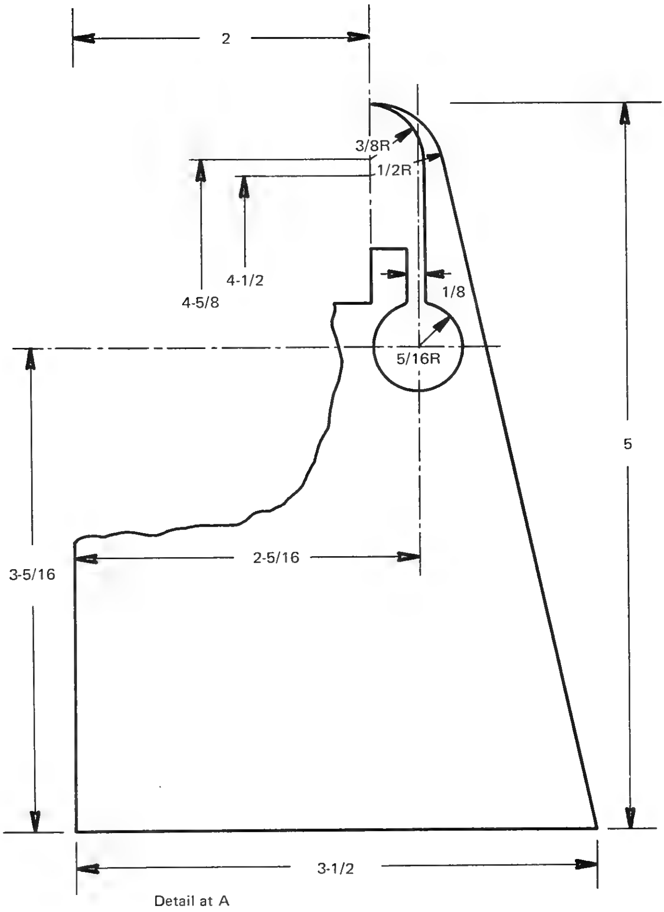

Figure 5. Details of the designed separation surface.

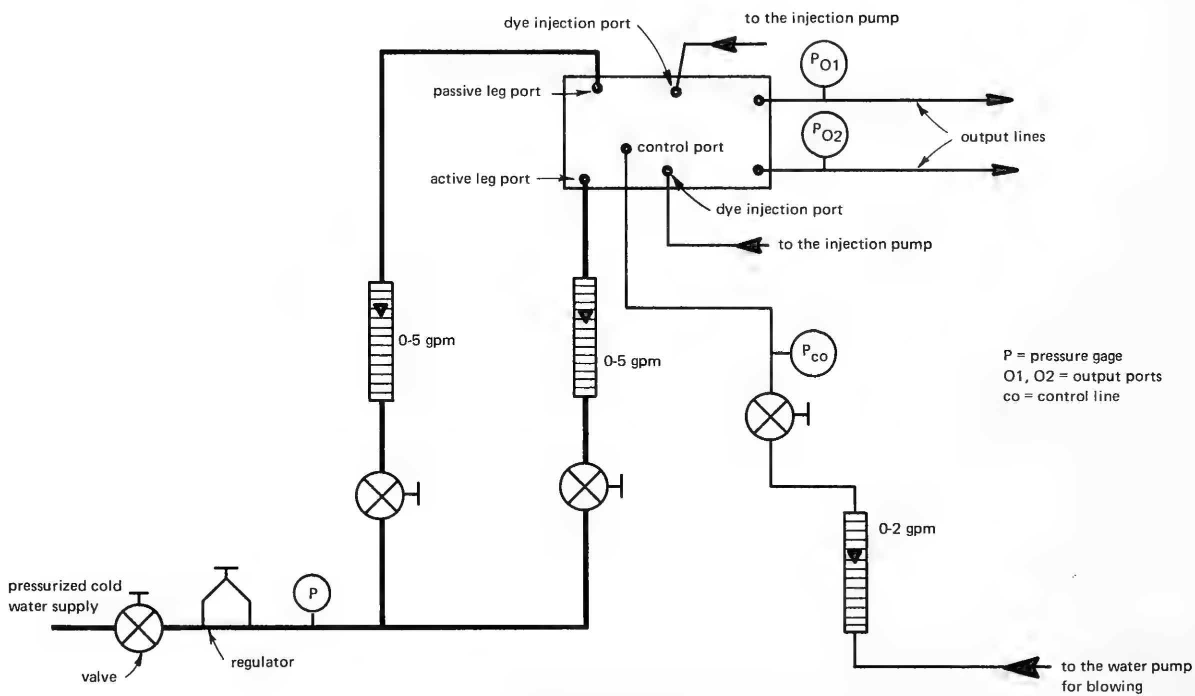

Figure 6. Schematic of the experimental elements test setup.

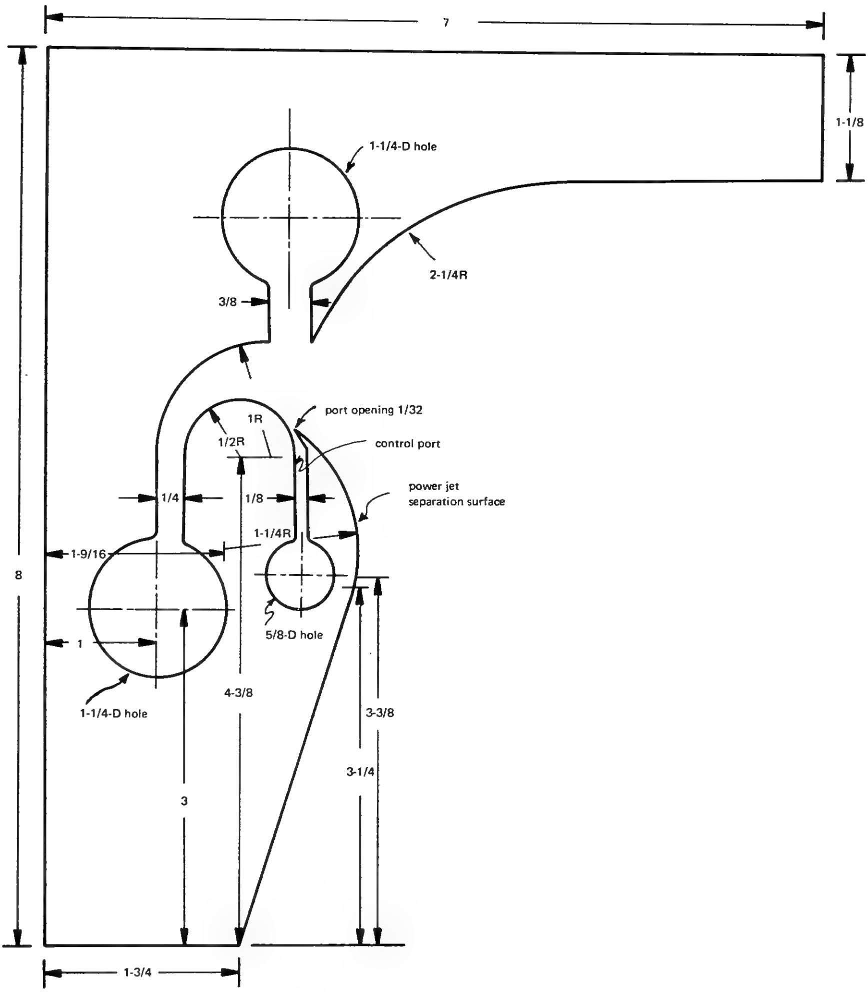

Figure 7. Sketch of the experimental element with the modifications.

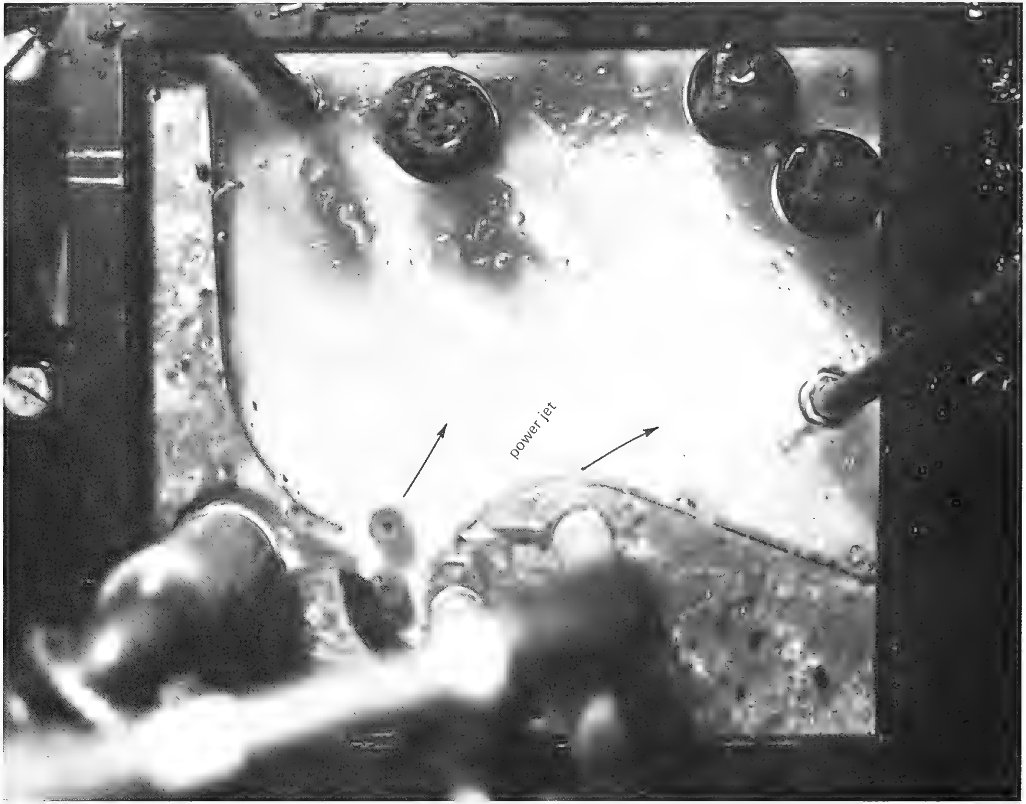

Figure 8. Flow pattern through the element, active leg flow of 4.0 gpm, passive leg flow of 3.5 gpm at zero control flow.

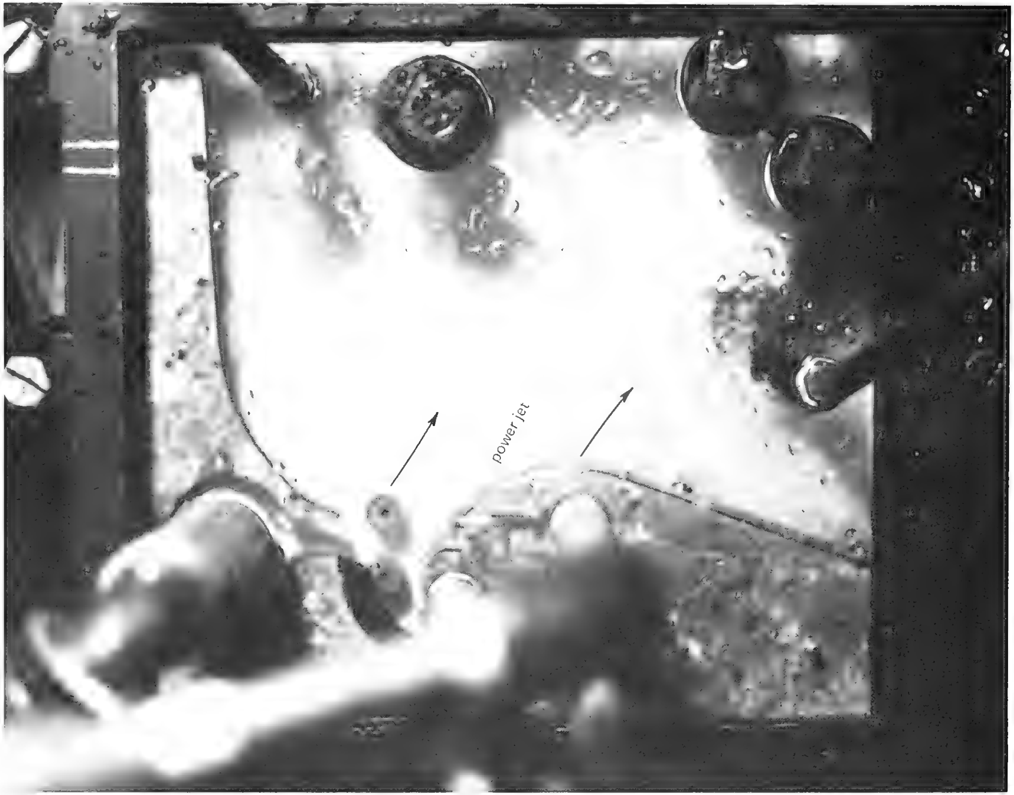

Figure 9. Flow pattern through the element at active leg flow of 4.0 gpm, passive leg flow of 3.5 gpm and control flow of 0.06 gpm.

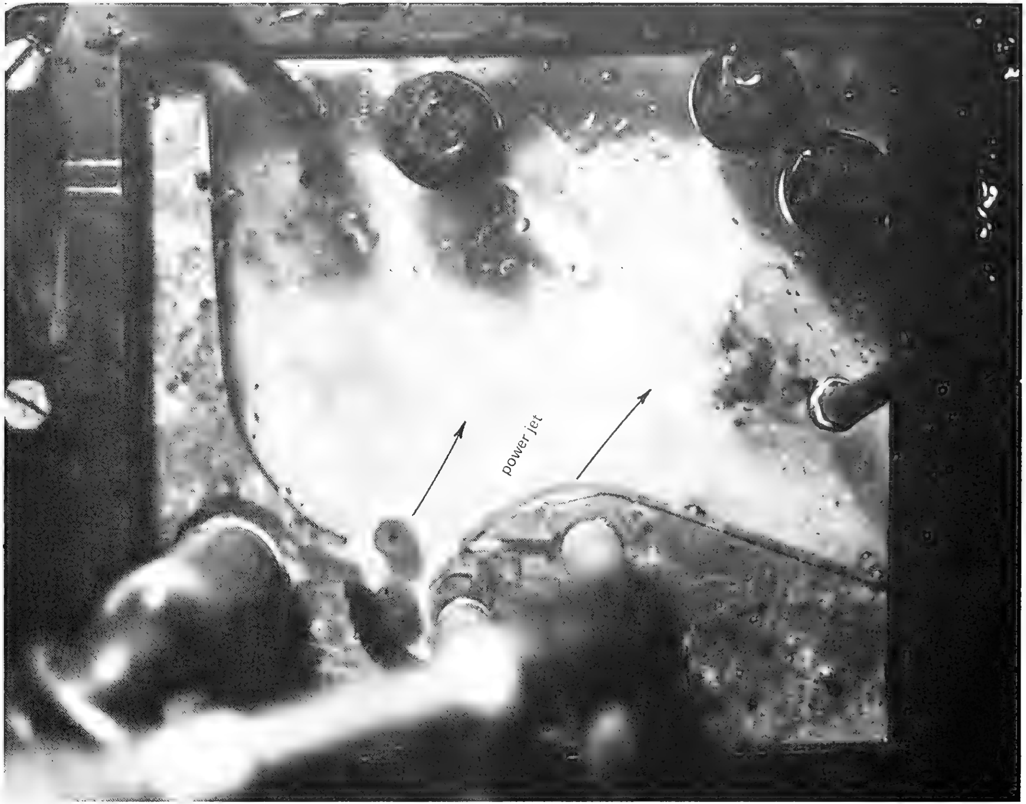

Figure 10. Flow pattern through the element at active leg flow of 4.0 gpm, passive leg flow of 3.5 gpm and control flow of 0.18 gpm.

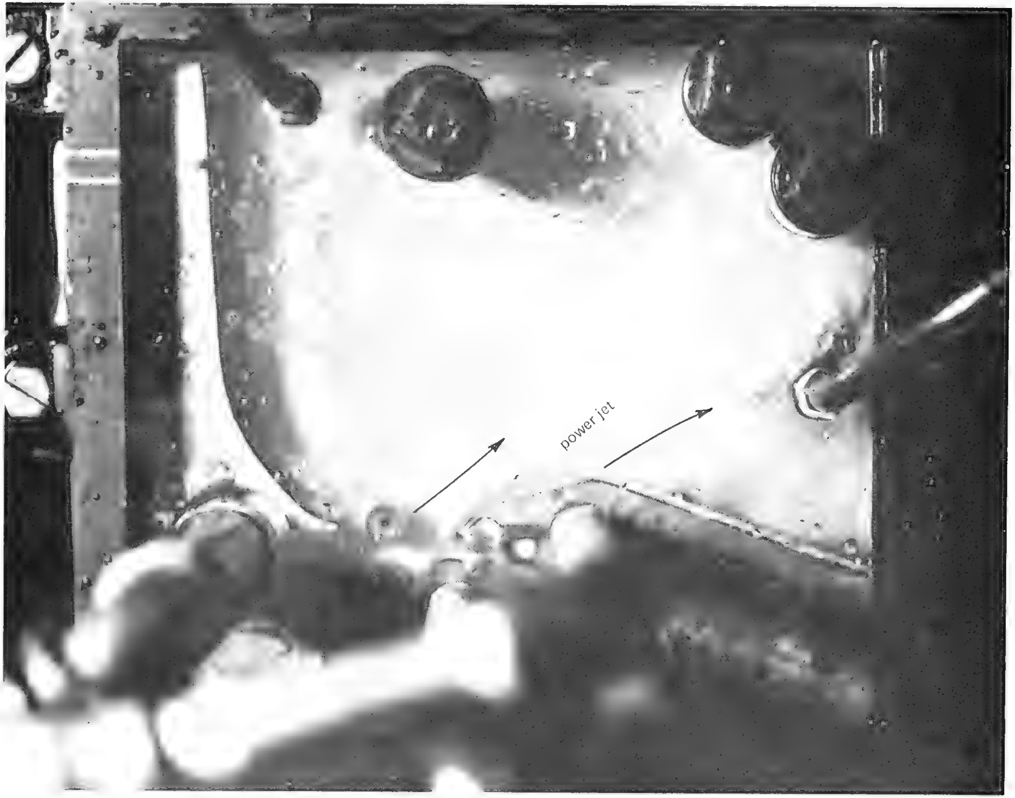

Figure 11. Flow pattern through the element at active leg flow of 3.0 gpm, passive leg flow of 3.0 gpm and zero control flow.

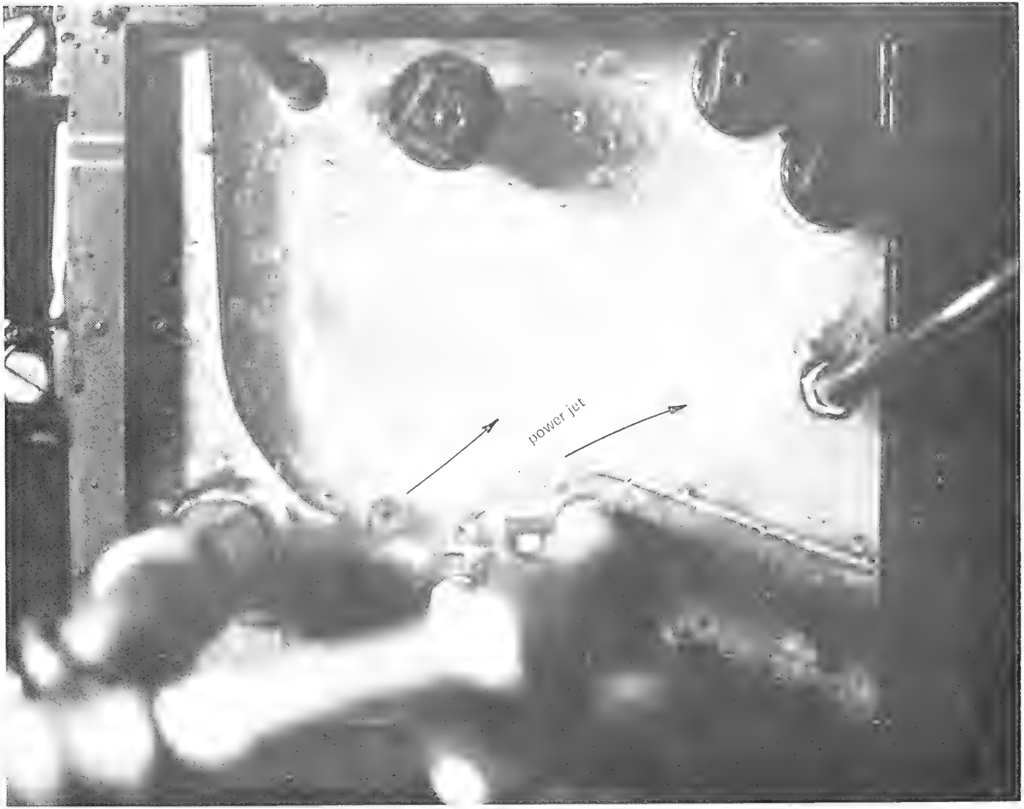

Figure 12. Flow pattern through the element at active leg flow of 3.0 gpm, passive leg flow of 3.0 gpm and control flow of 0.12 gpm.

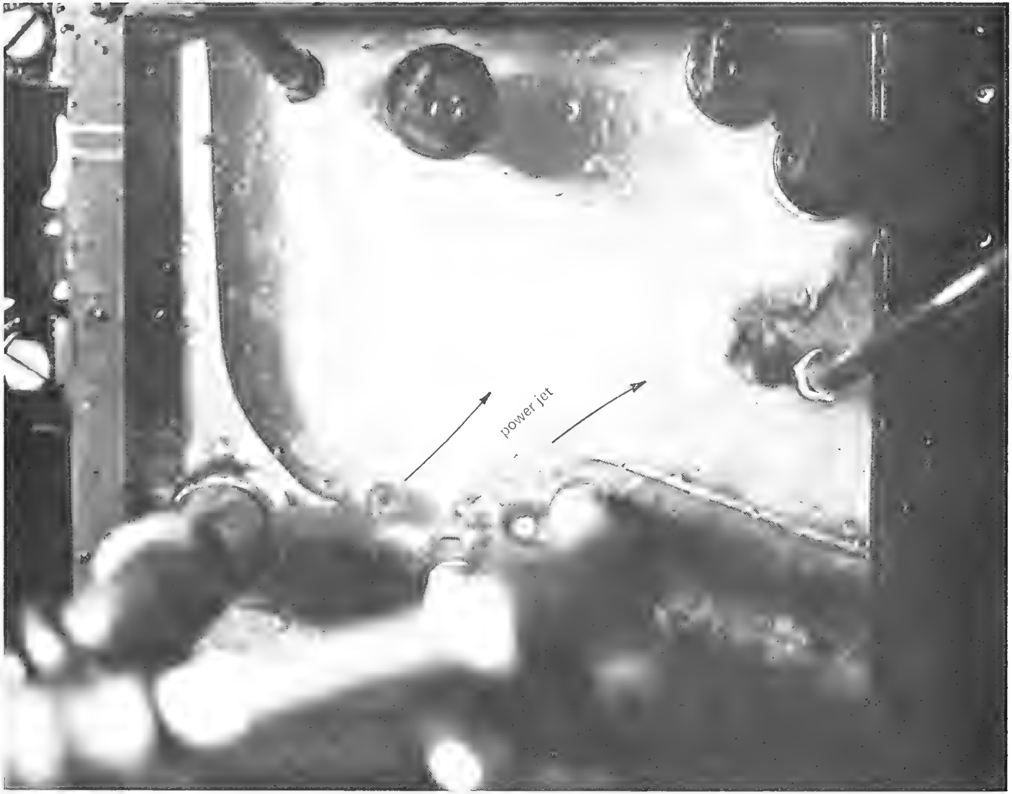

Figure 13. Flow pattern through the element at active leg flow of 3.0 gpm, passive leg flow of 3.0 gpm and control flow of 0.24 gpm.

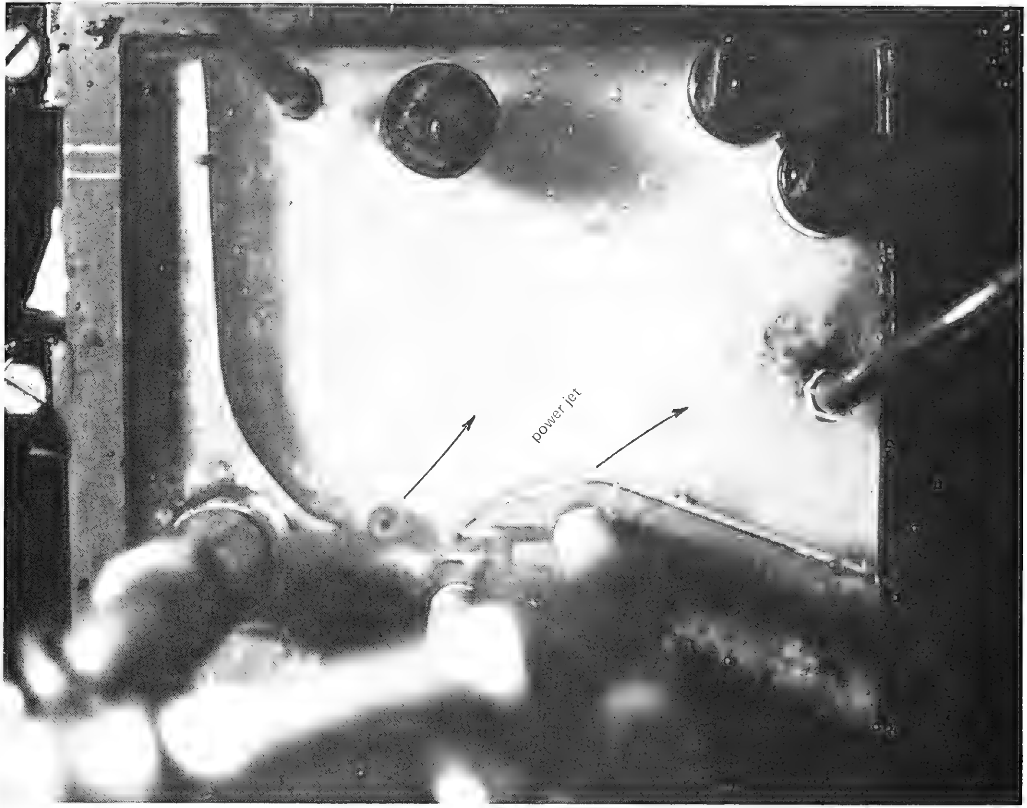

Figure 14. Flow pattern through the element at active leg flow of 4.75 gpm, passive leg flow of 3.5 gpm and zero control flow.

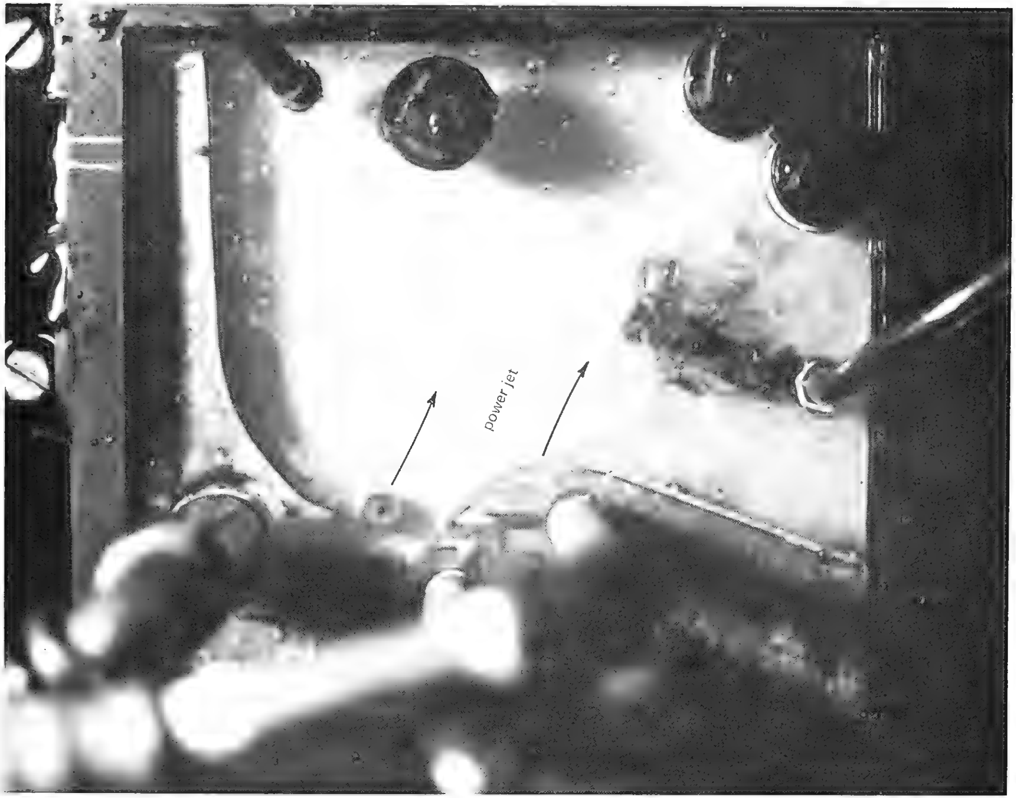

Figure 15. Flow pattern through the element at active leg flow of 4.75 gpm, passive leg flow of 3.5 gpm and control flow of 0.18 gpm.

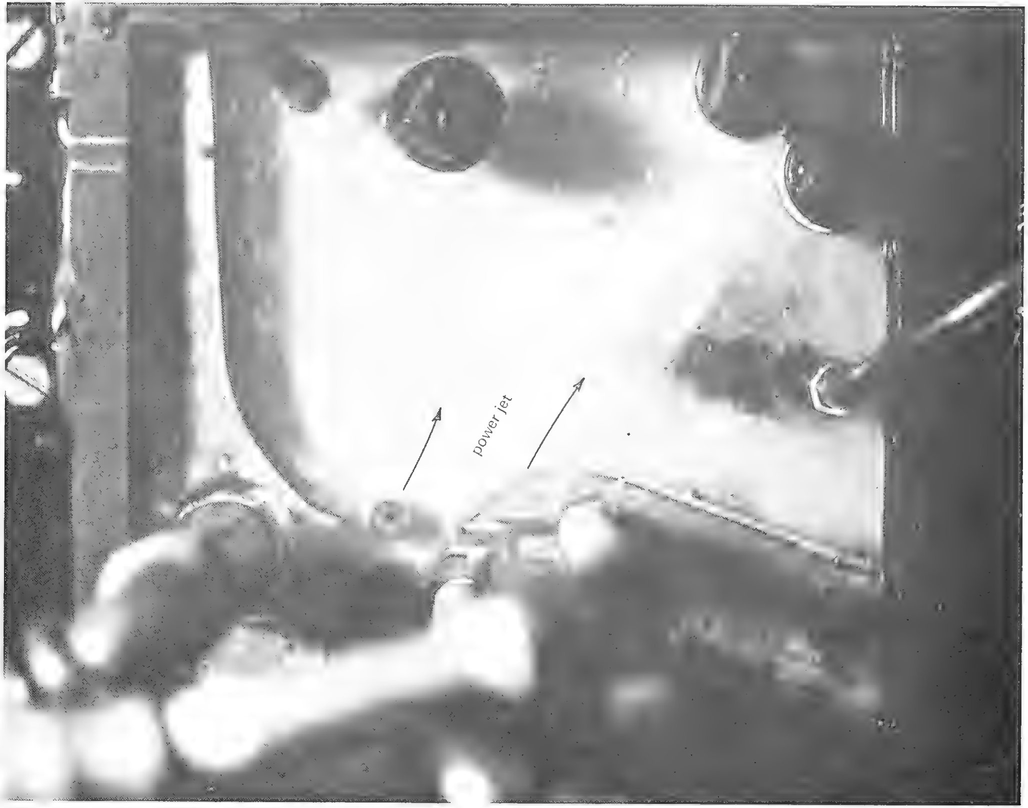

Figure 16. Flow pattern through the element at active leg flow of 4.75 gpm, passive leg flow of 3.5 gpm and control flow of 0.24 gpm.

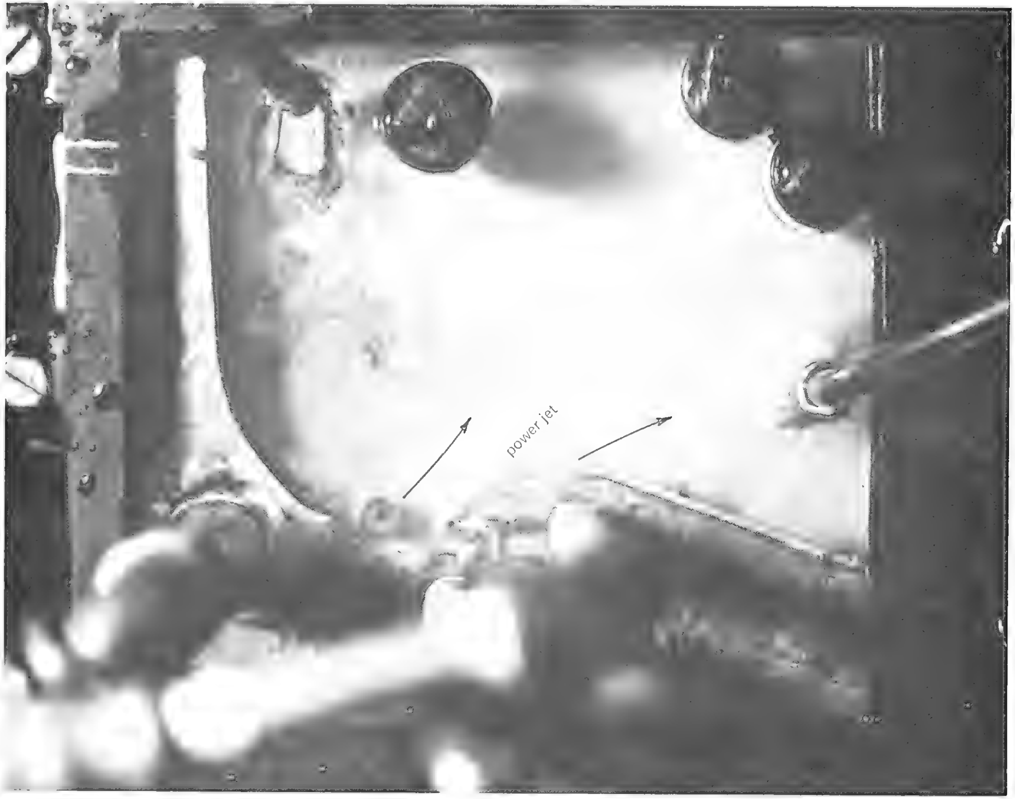

Figure 17. Flow pattern through the element at active leg flow of gpm, passive leg flow of gpm and zero control flow.

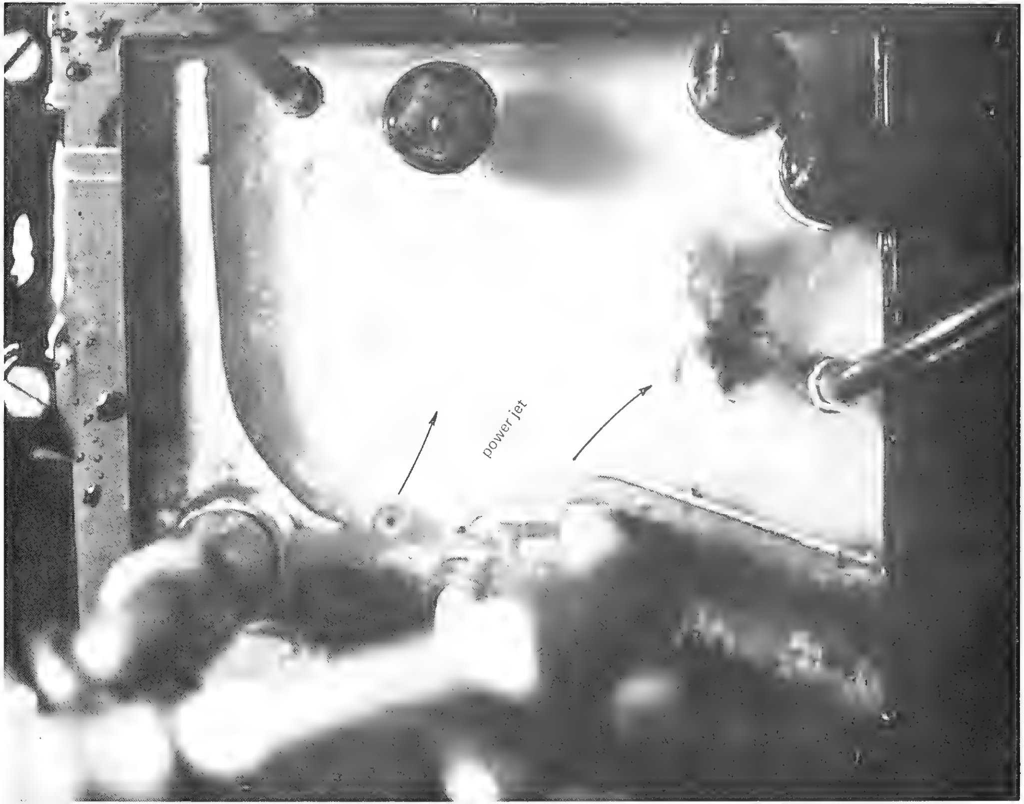

Figure 18. Flow pattern through the element at active leg flow of 5.0 gpm, passive leg flow of 4.0 gpm and control flow of 0.18 gpm.

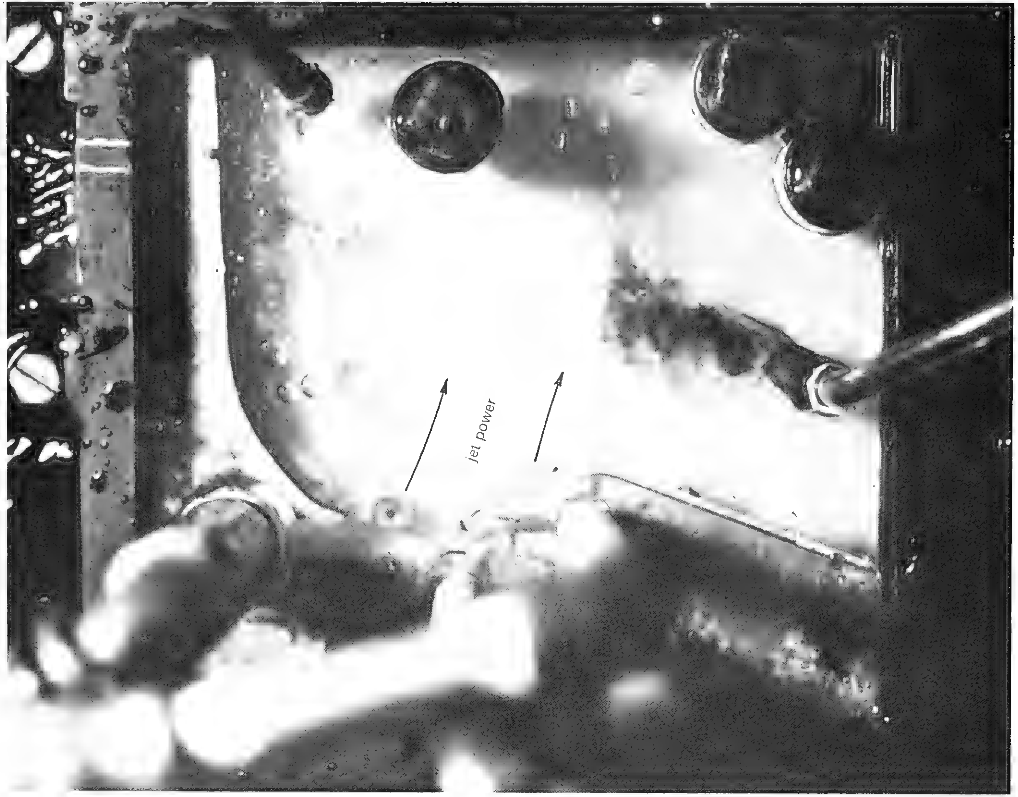

Figure 19. Flow pattern through the element at active leg flow of 5.0 gpm, passive leg flow of 4.0 gpm and control flow of 0.36 gpm.

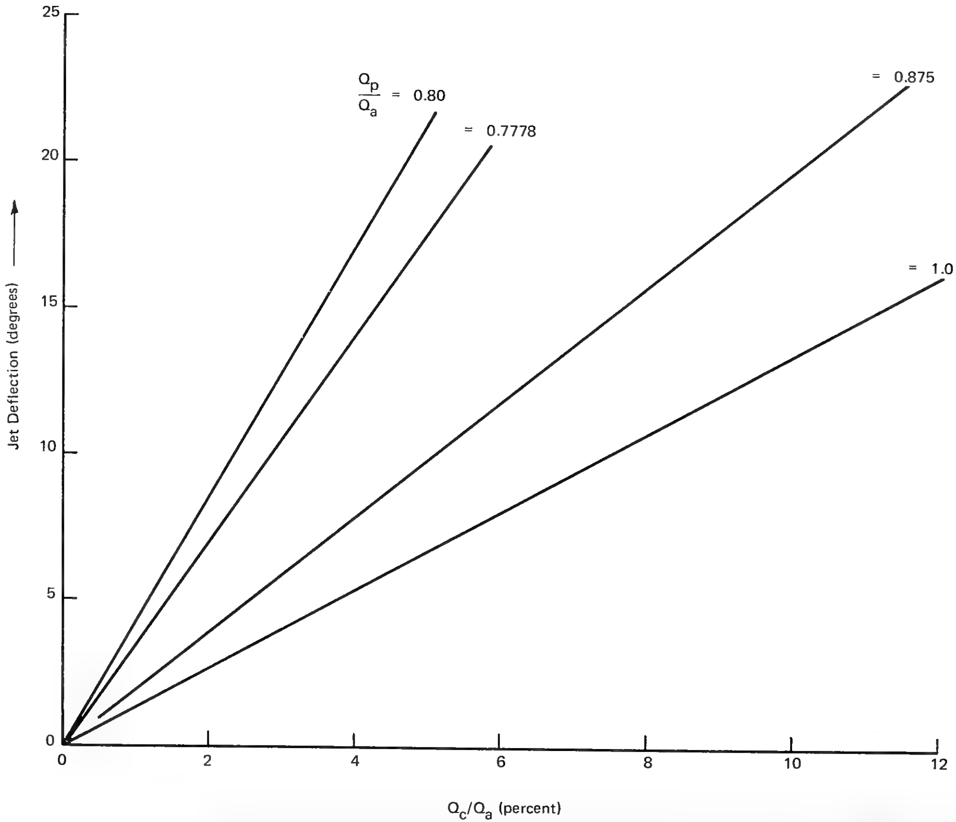

Figure 20. Power jet deflection characteristics of the element.

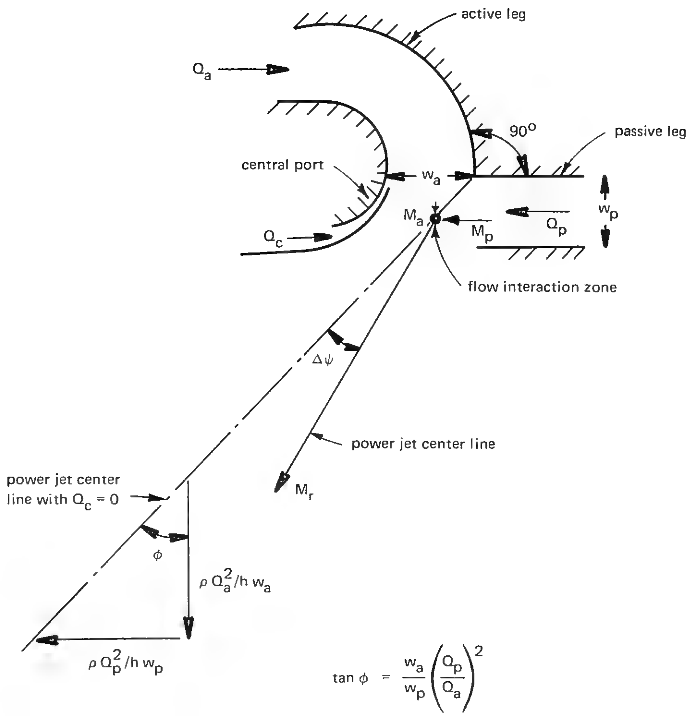

Figure 21. A schematic illustrating the double leg elbow amplifier theory.

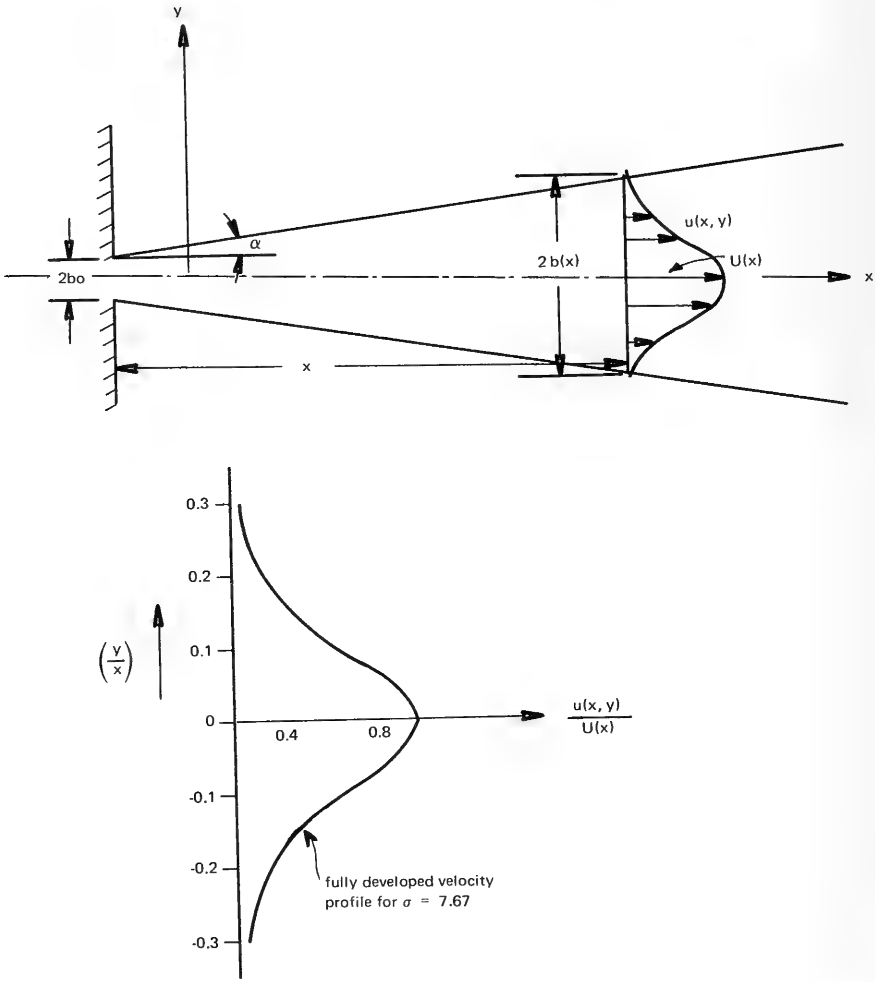

Figure 22. Submerged jet details.

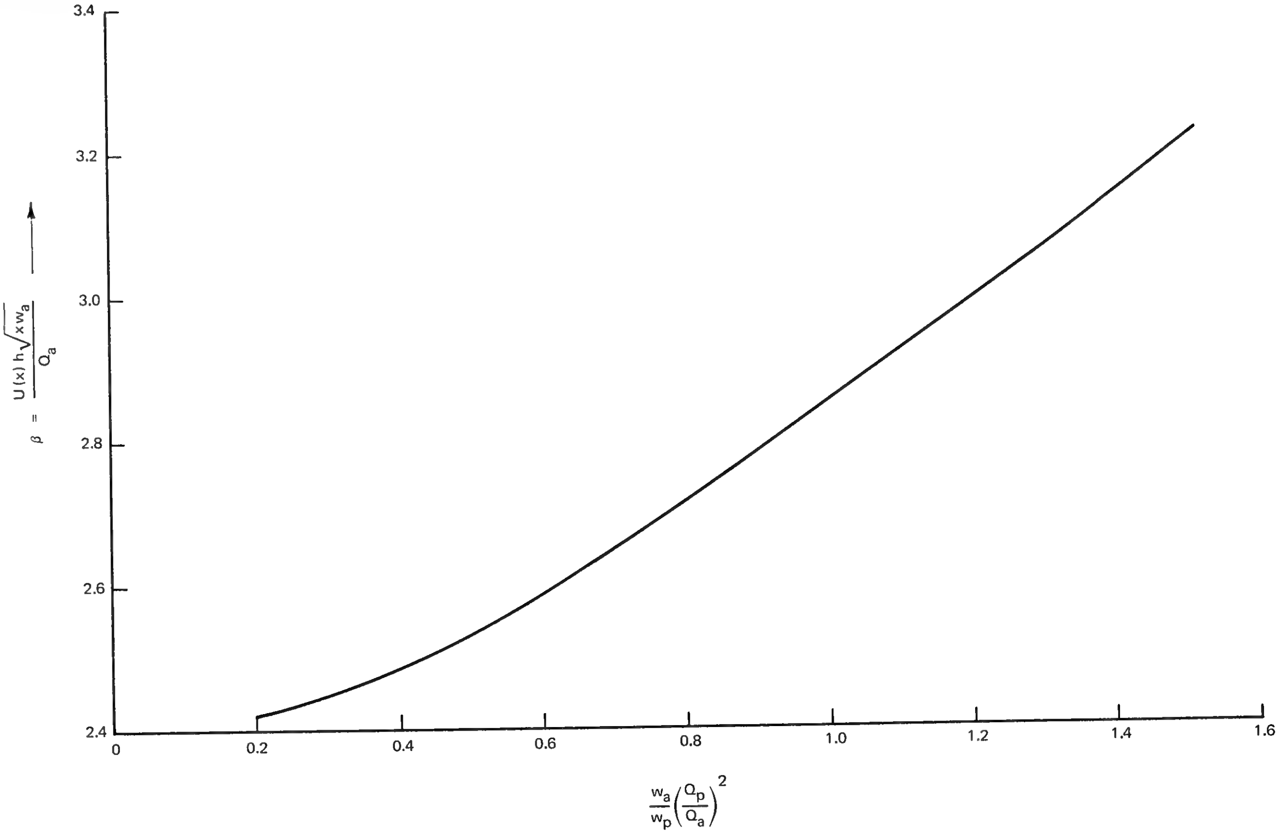

Figure 23. Solution of Equation 11.

$$w_o = x\,\Delta\psi_{max} = x\,\frac{S}{57.3}\left(\frac{Q_c}{Q_a}\right)_{max}$$

coordinates of Point A are $\left[x_o, -x_o\left(\frac{\Delta\psi_{max}}{2} + \Delta\psi\right)\right]$

coordinates of Point B are $\left[x_o, x_o\left(\frac{\Delta\psi_{max}}{2} - \Delta\psi\right)\right]$

coordinates of Point C are $\left[x_o, x_o\left(\frac{3}{2}\,\Delta\psi_{max} - \Delta\psi\right)\right]$

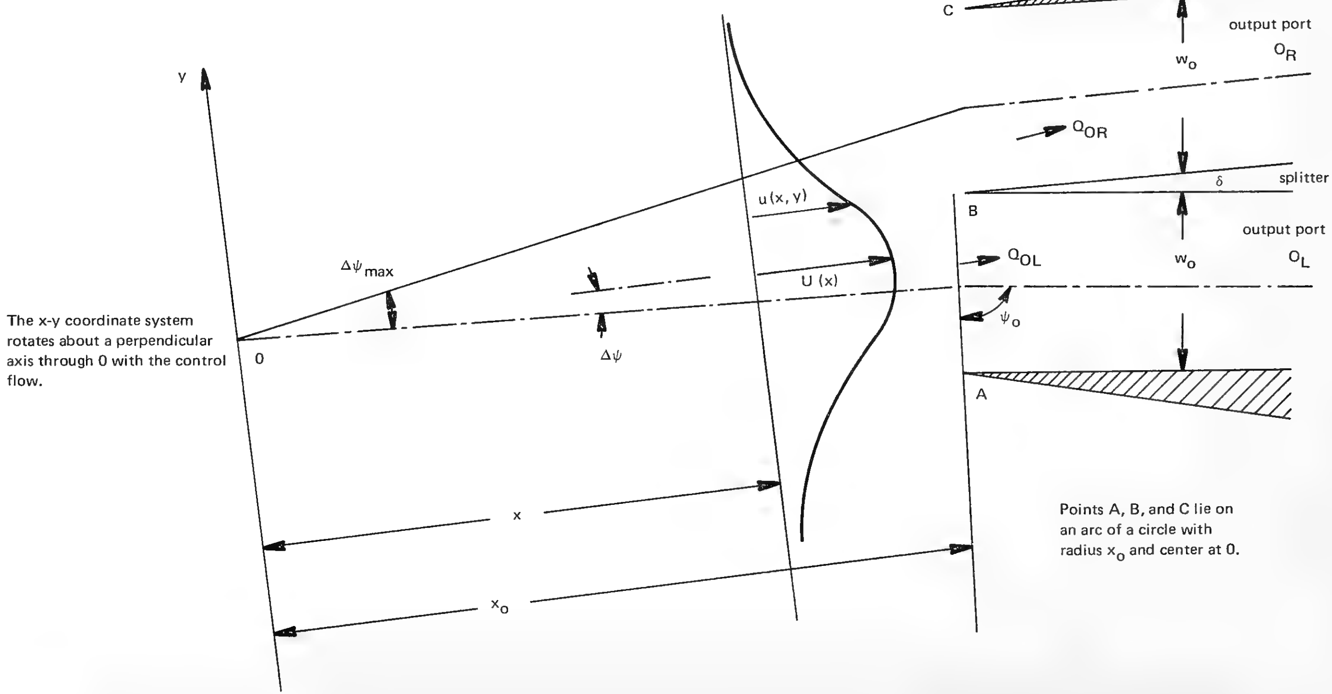

Figure 24. A sketch showing the flow through the output ports.

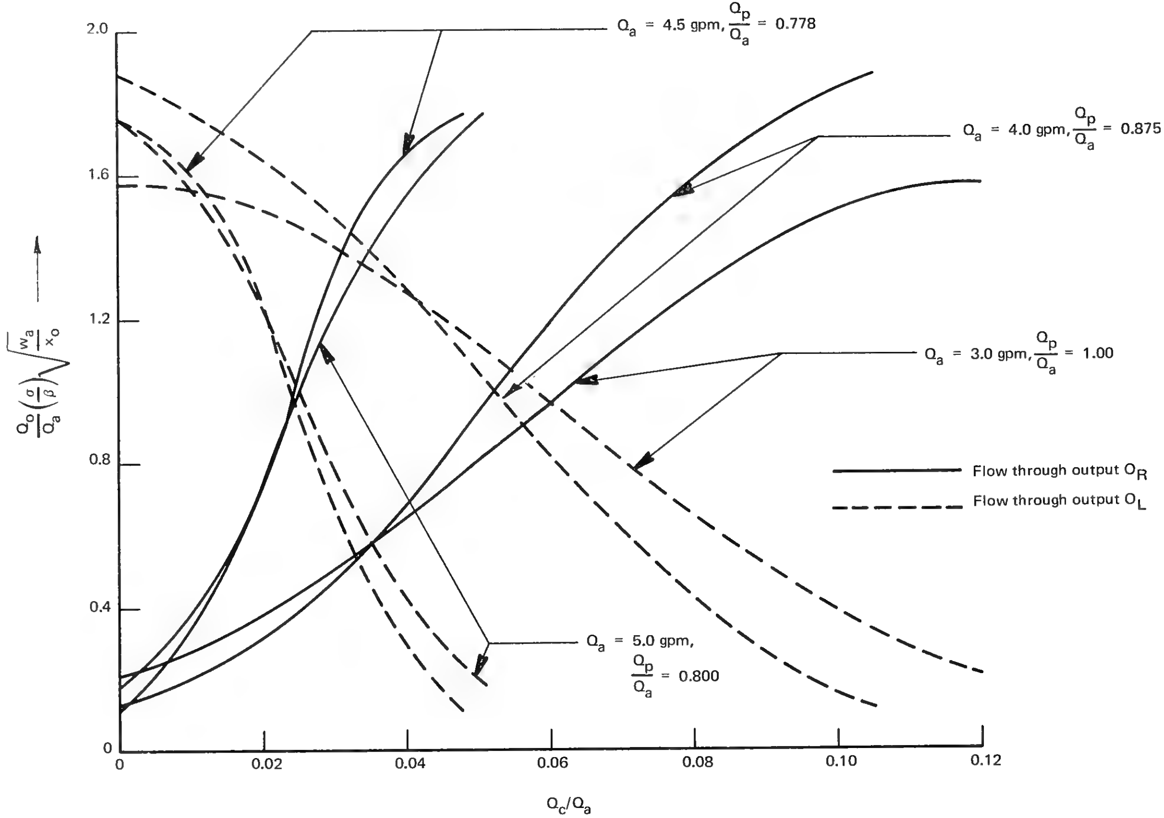

Figure 25. Output flow versus control flow characteristics.

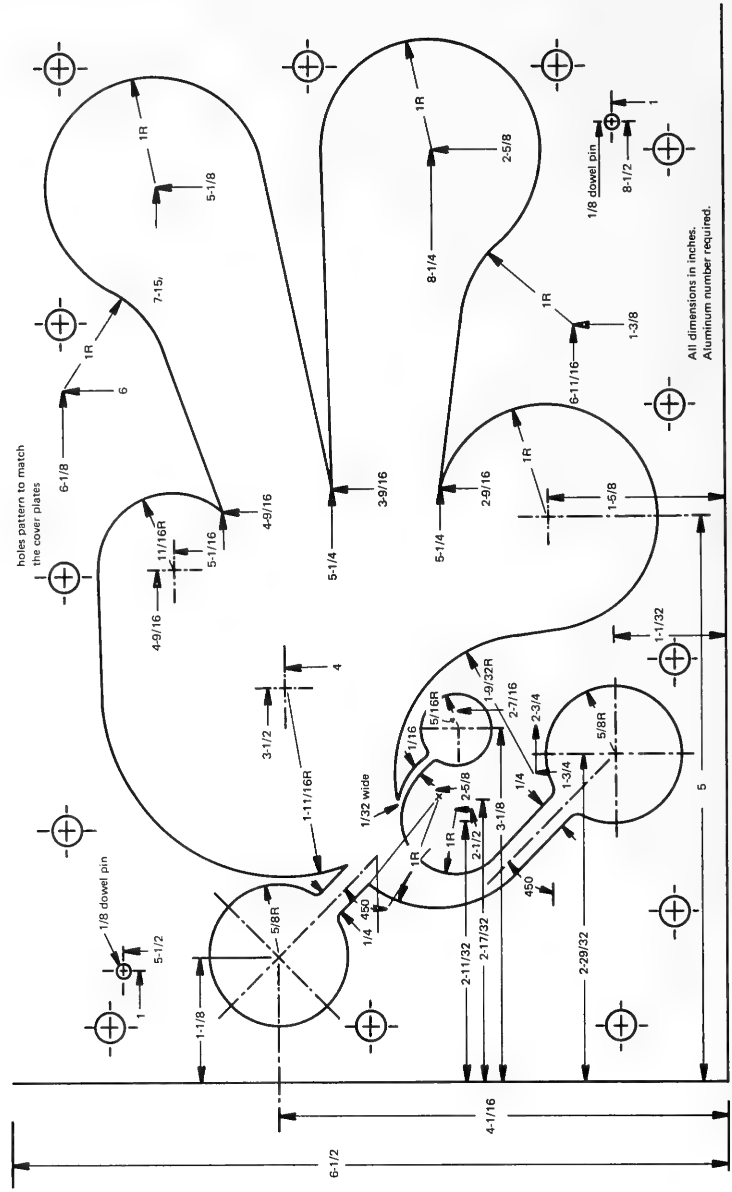

Figure 26. Fluid amplifier element.

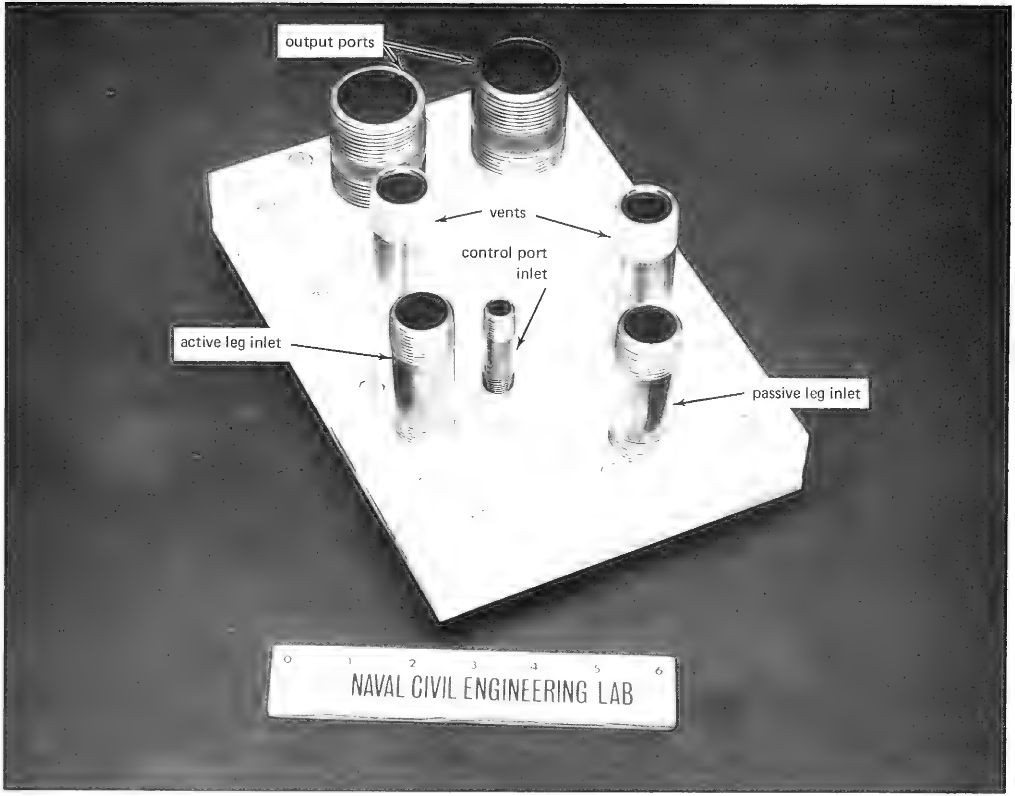

Figure 27. Assembled amplifier before testing.

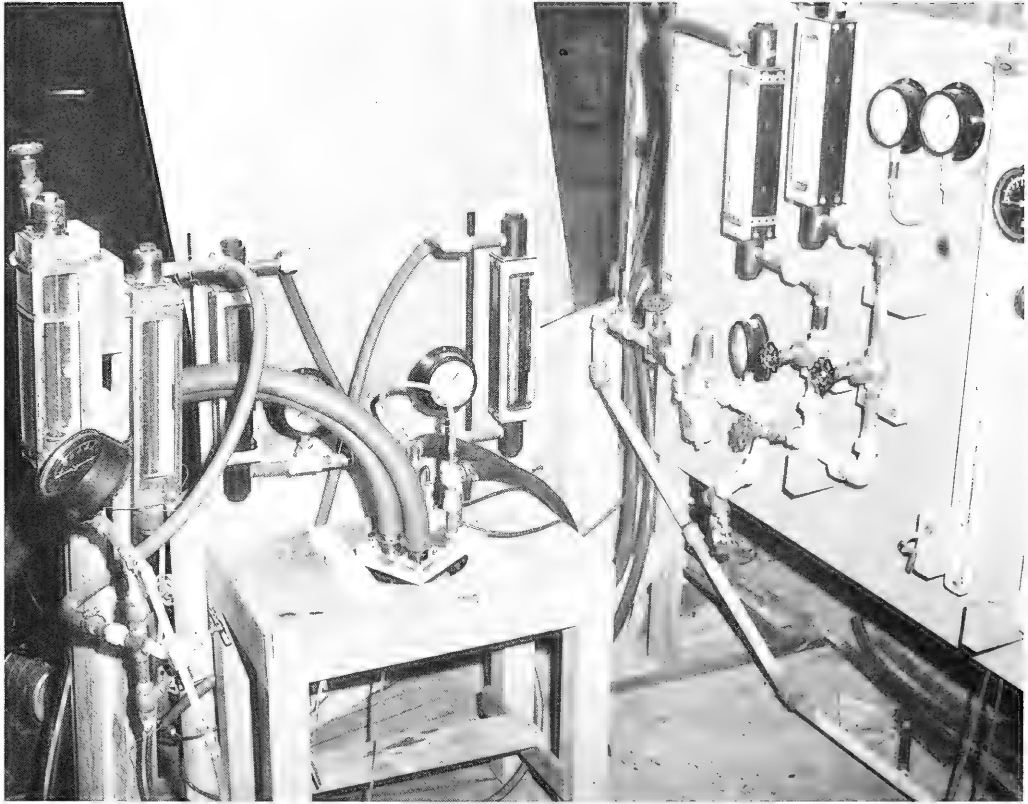

Figure 28. Amplifier undergoing tests.

Figure 29. Flow pattern through the amplifier with zero control.

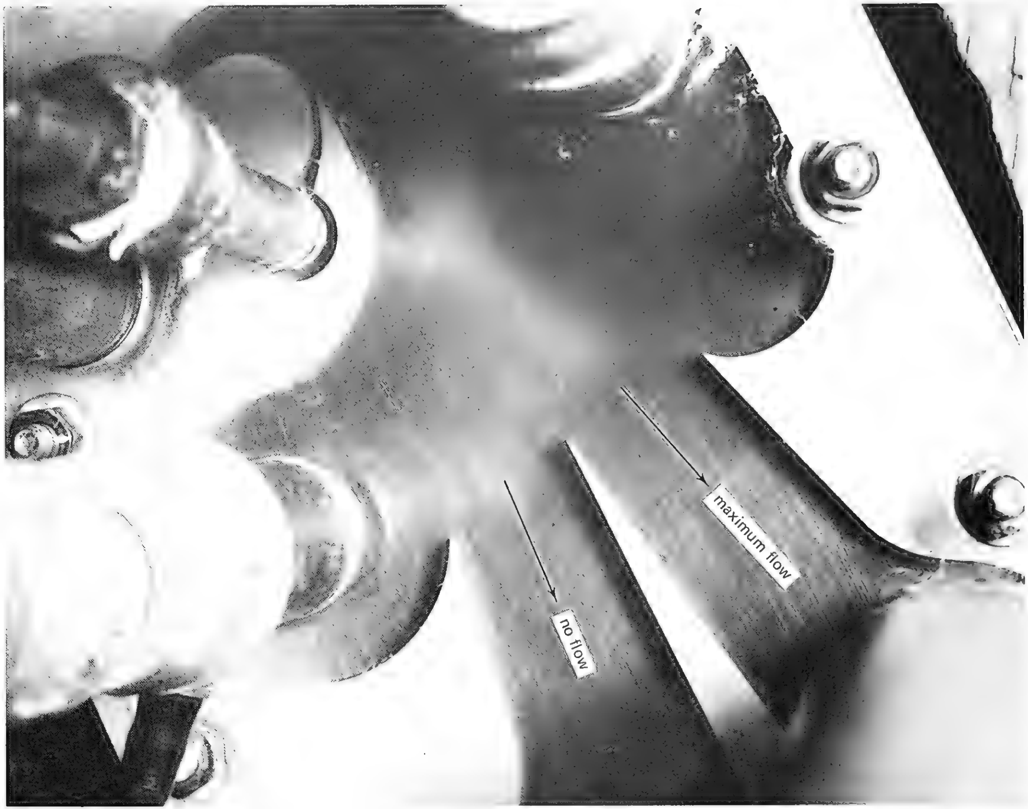

Figure 30. Flow pattern through the amplifier with 0.267 gpm of control flow.

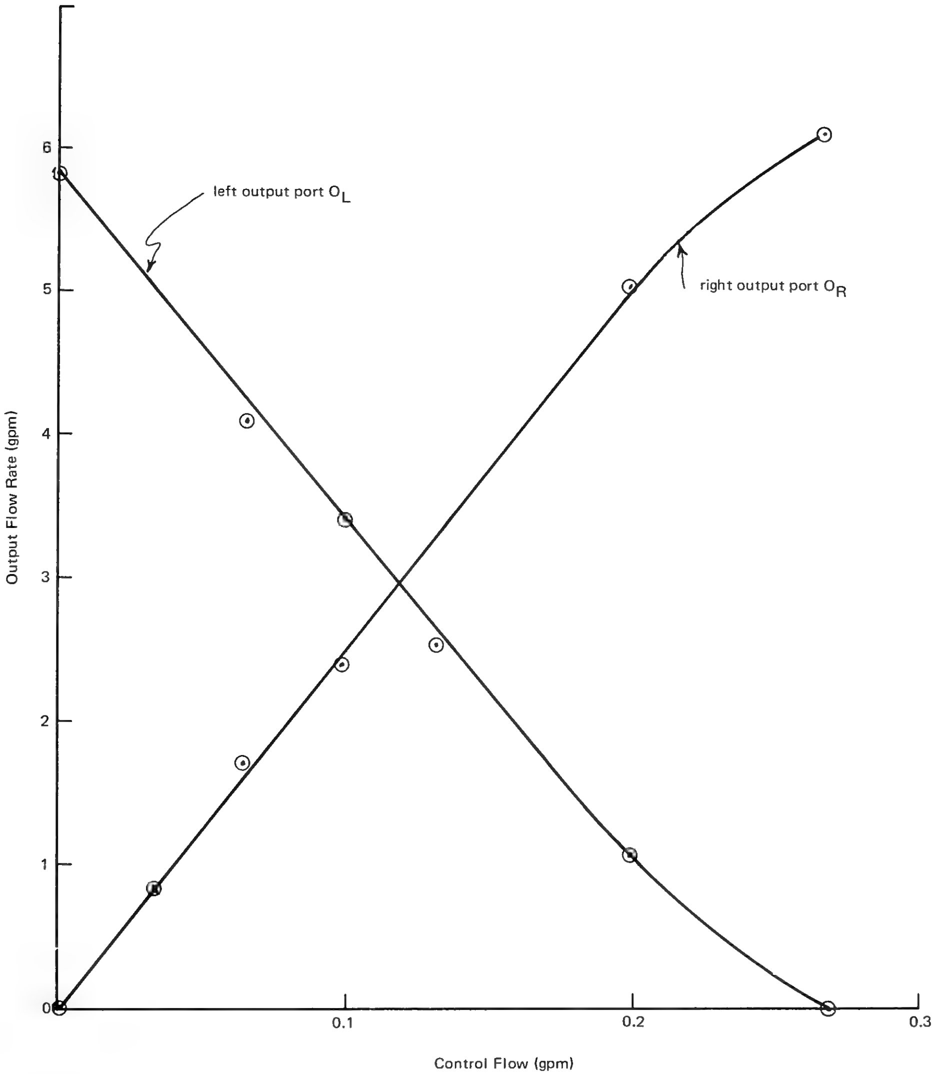

Figure 31. Output flow characteristics of the amplifier.

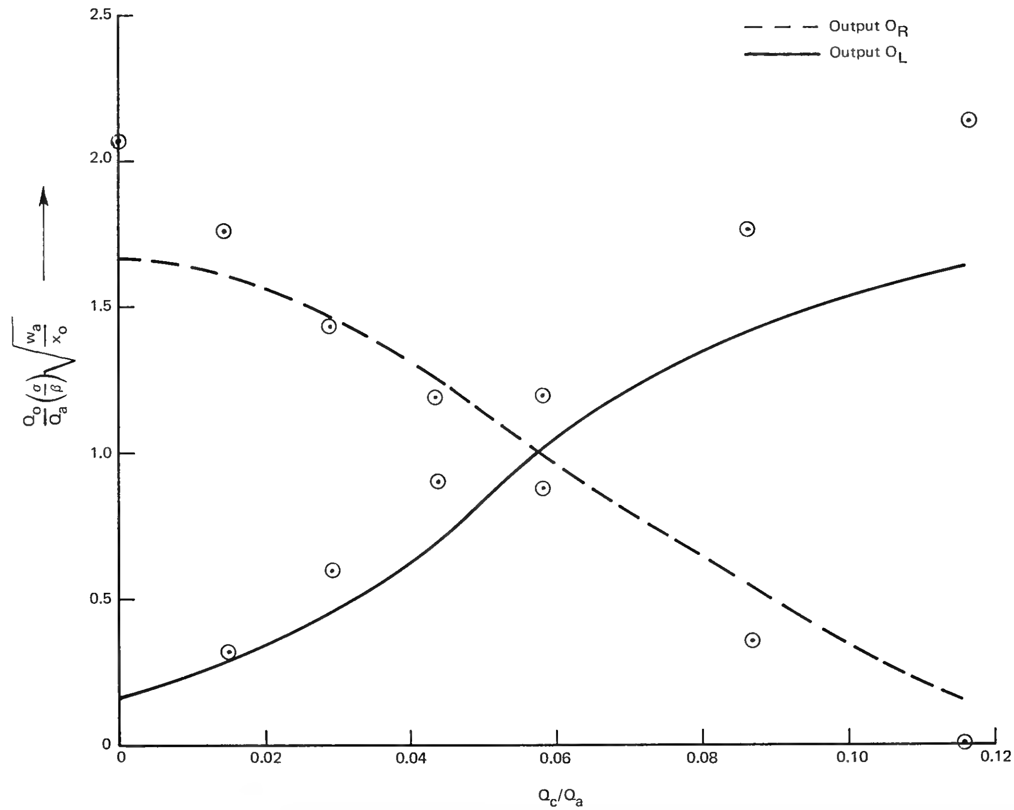

Figure 32. Comparison of the experimental and theoretical dimensionless output flow characteristics.

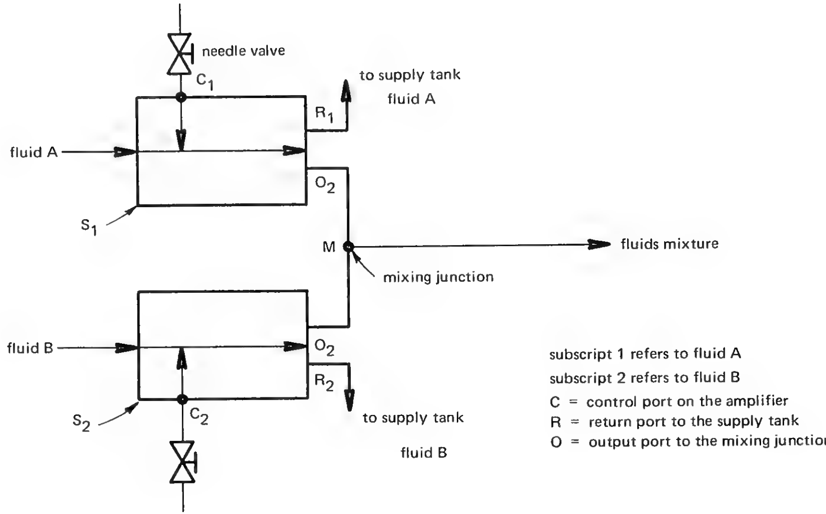

Figure 33. Manually operable fluidic mixing system.

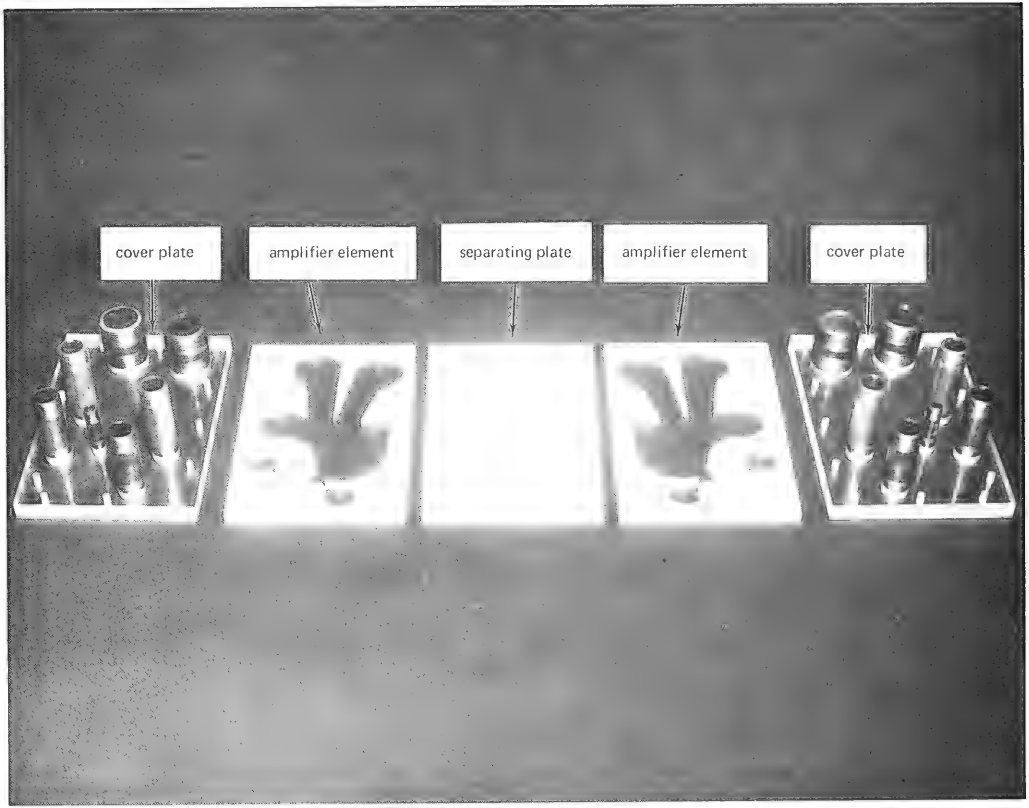

Figure 34. Mixing amplifier components.

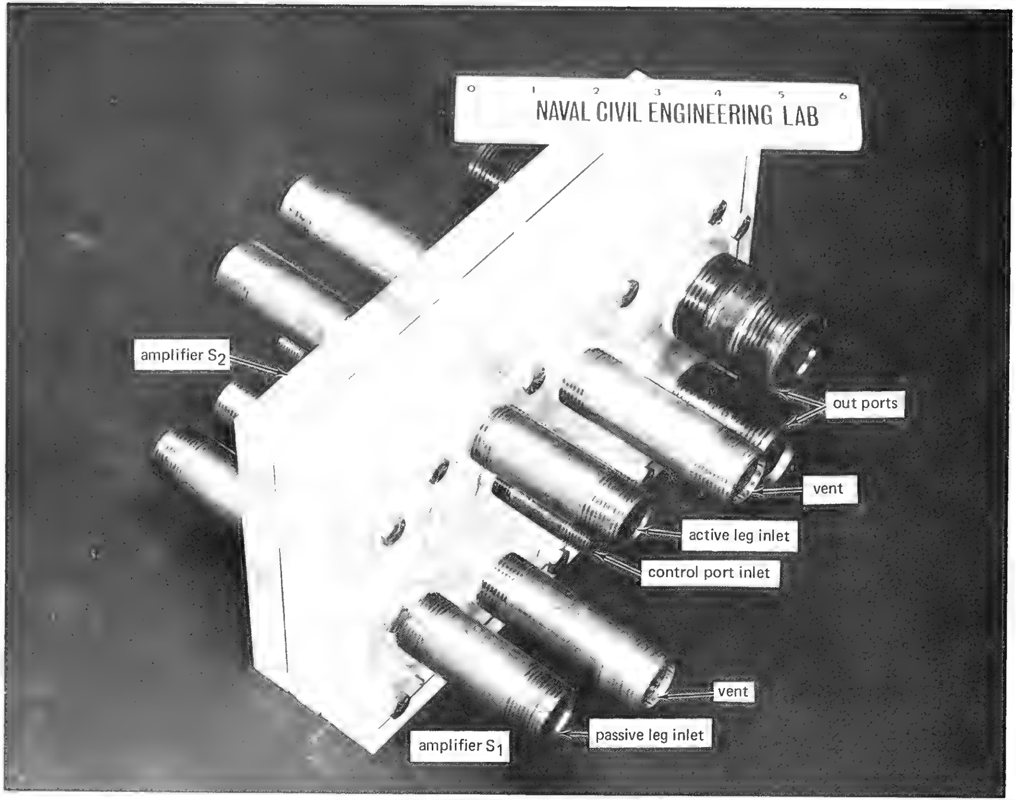

Figure 35. Assembled mixing element before tests.

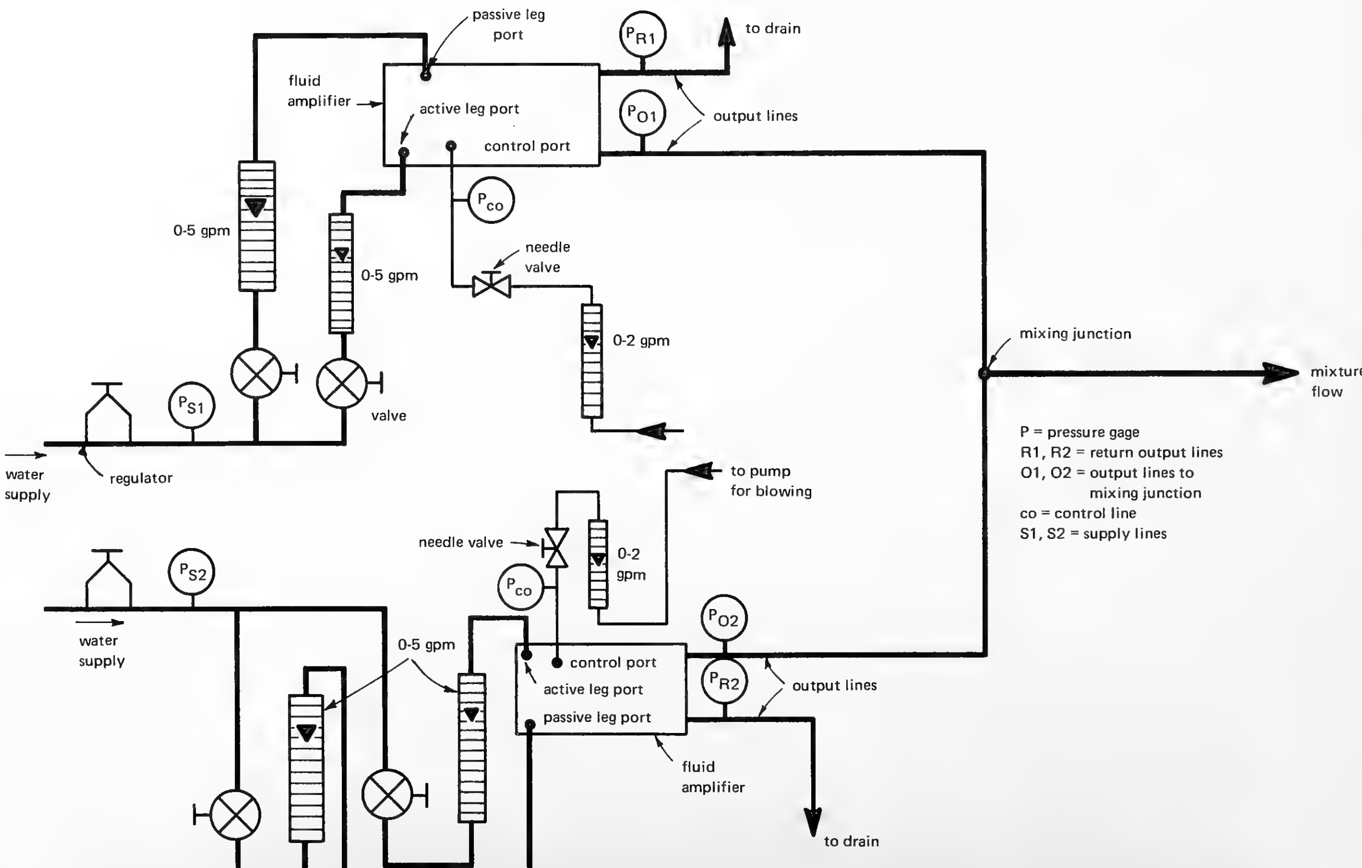

Figure 36. Schematic of the mixing system test setup.

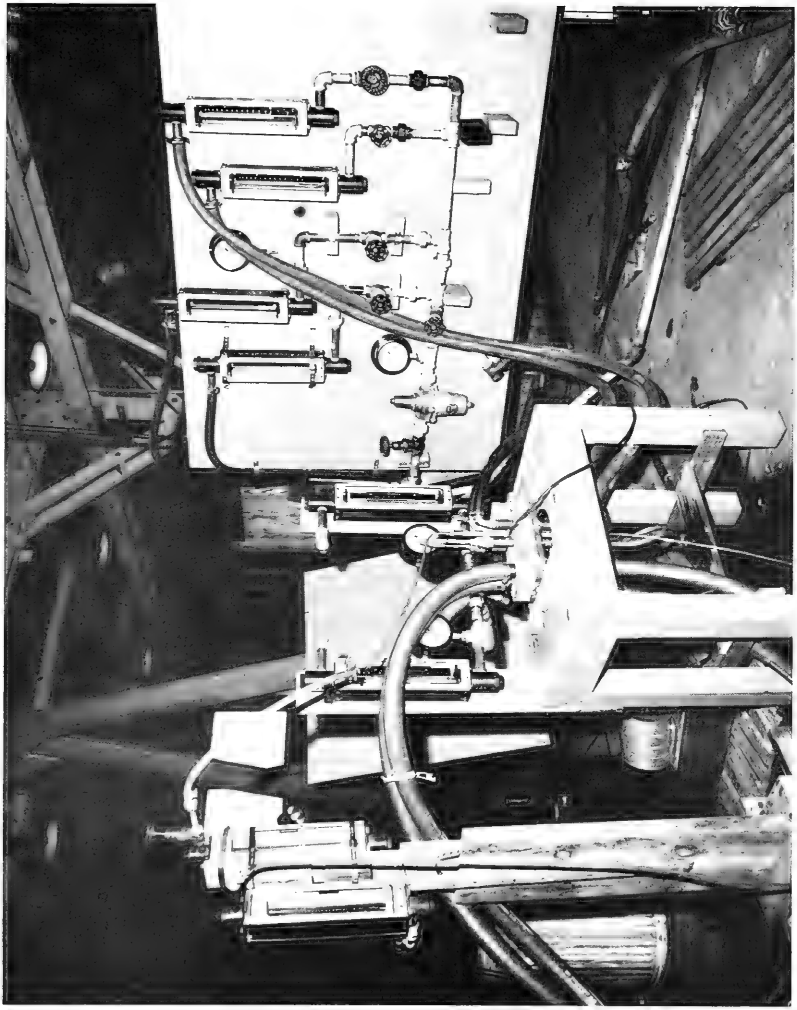

Figure 37. Mixing system test setup.

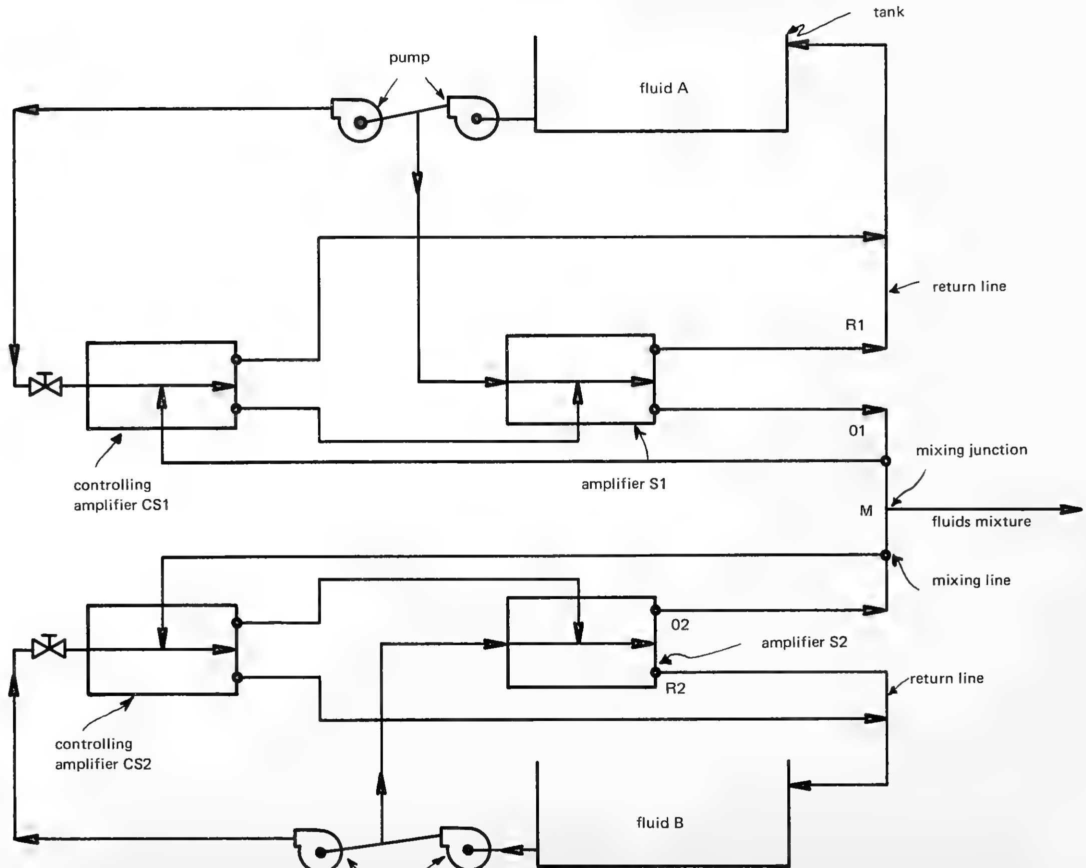

Figure 38. Automated mixing systems designed to mix two fluids.

REFERENCES

1. Naval Civil Engineering Laboratory. Technical Note N-1056: Fluidic devices for mixing two fluids - feasibility study, by D. Pal. Port Hueneme, California, Sep 1969.

2. Naval Civil Engineering Laboratory. Technical Note N-1150: A fluidic system for mixing two fluids - development study, by D. Pal. Port Hueneme, California, Feb 1971.

3. O. G. Brown and A. N. Harris "Turbulent flow of water in plane curved channels of finite depth", presented at the ASME Winter Meeting, New York, 1962.

4. Salman Eskinazi and Hsuan Yeh. An investigation on fully developed turbulent flows in a curved channel. Journal of the Aerospace Sciences, Vol 23, No. 1, Jan 1956, pp. 23-24, 75.

5. H. A. Curtiss, O. G. Feil, and D. J. Liquirnik. Separated flow in curved channels with secondary injection. In Proceedings of the Fluid Amplification Symposium, Washington, D. C., May 1964, Vol, IV, Harry Diamond Laboratories, pp. 21-50.

6. H. A. Curtiss and D. J. Liquirnik . Research studies in proportional fluid state control components. Final Report on Contract DA36-034-ORD-3722 RD, Redstone Arsenal, Alabama (Giannini Controls Corp.).

7. Herman Schlichting. Boundary layer theory. McGraw Hill Book Company, Inc., New York, Fourth Edition, pp. 590-613.

8. Harry Diamond Laboratories. Report No. R-RCD-72-1: Hydraulic-fluidic tests on G. E.proportional amplifier, by Fernando Villarroel, Washington, D. C., 20438.

DISTRIBUTION LIST

SNDL Code	No. of Activities	Total Copies	
–	1	12	Defense Documentation Center
–	1	1	Director of Navy Laboratories
FKAIC	1	3	Naval Facilities Engineering Command
FKNI	6	6	NAVFAC Engineering Field Division
FKN5	9	9	Public Works Centers
FA25	1	1	Public Works Center
–	9	9	RDT&E Liaison Officers at NAVFAC Engineering Field Divisions and Construction Battalion Centers
–	301	301	NCEL Special Distribution List No. 8 for persons and activities interested in reports on Mechanical Systems

Natick Labs *
Kansas St.
Natick, MA 01761

Public Works Officer
Boston Naval Shipyard
Boston, MA 02129

Public Works Officer
Naval Hospital, Boston
Chelsea, MA 02150

Dr. E. M. Lenoe
Army Materials & Mechanics Research Center
Bldg 39, Room 412
Arsenal Street
Watertown, MA 02172

Public Works Officer
Naval Air Station
South Weymouth, MA 02190

LCDR David A. Cacchione, USN
Office of Naval Research, Broff
495 Summer Street
Boston, MA 02210

Public Works Officer
Naval Facility
Nantucket, MA 02554

Public Works Officer
Naval Air Station
Quonset Point, RI 02819

* All addressees receive one copy unless otherwise indicated.

Commanding Officer (Code 200)
Navy Public Works Center
Naval Base
Newport, RI 02840

Commanding Officer
Naval Supply Depot
Newport, RI 02840

President
Naval War College
Code 22
Newport, RI 02840

Commanding Officer
U.S. Naval Station
Naval Base
Newport, RI 02840

Staff Civil Engineer
Naval Supply Center
Newport, RI 02840

Mr. S. Milligan
SB 322
Naval Underwater Systems Center
Newport, RI 02844

Public Works Officer
Naval Underwater Systems Center
Newport, RI 02844

Commanding Officer
CBC Technical Library
Naval Construction Battalion Center
Davisville, RI 02854 (2 copies)

Public Works Officer
Portsmouth Naval Shipyard
Portsmouth, NH 03801

Public Works Officer
U.S. Naval Disciplinary Command
Portsmouth, NH 03801

Public Works Officer
Naval Air Station
Brunswick, ME 04011

Public Works Officer
Naval Radio Station (T), Cutler
East Machias, ME 04630

Facilities Officer
Code NA 2
New London Laboratory
Naval Underwater Systems Center
New London, CT 06320

Public Works Department
Box 400
Naval Submarine Base, New London
Groton, CT 06340

Commanding General
U. S. Army Electronics Command
Attn: AMSEL-GG-TD
Fort Monmouth, NJ 07703

Public Works Officer
Naval Air Propulsion Test Center
Trenton, NJ 08628

Public Works Officer
Naval Air Station
Lakehurst, NJ 08733

Commanding Officer
Mobile Construction Battalion 74
FPO New York 09501

Public Works Officer
U. S. Naval Support Force Antarctica
FPO New York 09501

Commanding Officer
Amphibious Construction Battalion TWO
FPO New York 09501

Public Works Officer
U.S. Naval Activities, United Kingdom
FPO New York 09510

Public Works Officer
U.S. Naval Activities, United Kingdom Det.
FPO New York 09510

Public Works Officer
U. S. Naval Communication Station
FPO New York 09512

Public Works Officer
U. S. Naval Security Group Activity
FPO New York 09518

Public Works Officer
U. S. Naval Air Facility
FPO New York 09520

Public Works Officer
U.S. Naval Support Activity
FPO New York 09521

Director
European Branch-Atlantic Division
Naval Facilities Engineering Command
Naval Support Activity-Box 51
FPO New York 09521

Public Works Officer
U. S. Naval Air Facility
FPO New York 09523

Public Works Officer
U. S. Naval Communication Station
FPO New York 09525

Public Works Officer
U.S. Naval Control of Shipping Office
FPO New York 09526

Public Works Officer
U. S. Naval Medical Research Unit No. 3
FPO New York 09527

Public Works Officer
U.S. Navy Fleet Support Office
FPO New York 09532

LT Ronald A. Milner, CEC, USN
U. S. Naval Station
Box 9
FPO New York 09540

Public Works Officer
Morocco-U. S. Naval Training Command
Box 19
FPO New York 09544

Public Works Officer
U. S. Naval Communication Station
Box 41
FPO New York 09544

Public Works Officer
U.S. Navy Support Activity
FPO New York 09550

Public Works Officer
U.S. Naval Station
FPO New York 09551

Commanding Officer
U.S. Naval Hospital
FPO New York 09551

Public Works Officer
U. S. Naval Facility
FPO New York 09552

Public Works Officer
U. S. Naval Facility
FPO New York 09553

Public Works Officer
U.S. Naval Communication Station
FPO New York 09554

Public Works Officer
U.S. Naval Security Group Activity
FPO New York 09555

Public Works Officer
U. S. Naval Facility
FPO New York 09558

Public Works Officer
U. S. Naval Air Station
FPO New York 09560

Public Works Officer
U. S. Naval Station
FPO New York 09571

Public Works Officer
U. S. Naval Communication Station
FPO New York 09580

Public Works Officer
U. S. Naval Support Activity
FPO New York 09585

Public Works Officer
U. S. Naval Station
Box 25
FPO New York 09593

Public Works Officer
U. S. Naval Station
Box 6
FPO New York 09597

Public Works Officer
U. S. Naval Communication Station
APO New York 09843

Public Works Officer, Naval Station
136 Flushing Avenue
Brooklyn, NY 11251

Public Works Officer
Naval Strategic Systems Navigation Facility
Flushing & Washington Avenue
Brooklyn, NY 11251

Public Works Officer
U. S. Naval Hospital
St. Albans, LI, NY 11425

Public Works Officer
Naval Ships Parts Control Center
Mechanicsburg, PA 17055

Public Works Officer
Naval Air Development Center
Warminster, PA 18974

Public Works Officer
Naval Air Station
Willow Grove, PA 19090

Commanding Officer
Code 016A
Northern Division
Naval Facilities Engineering Command
Philadelphia, PA 19112

RDT&E Liaison Officer
Code 102 Northern Division
Naval Facilities Engineering Command
Philadelphia, PA 19112

Public Works Officer
Philadelphia Naval Shipyard
Philadelphia, PA 19112

Commanding Officer
Naval Station
Philadelphia, PA 19112

Public Works Officer
Naval Air Engineering Center
Philadelphia, PA 19112

Public Works Officer
Naval Hospital
17th Street & Pattison Avenue
Philadelphia, PA 19145

Public Works Officer
National Naval Medical Center
Bethesda, MD 20014

Mr. R. B. Allnutt
Code 1706
Naval Ship Research & Development Center
Bethesda, MD 20034

Head Facilities & Industrial Department
Code 54
Carderock Laboratory
Naval Ship Research & Development Center
Bethesda, MD 20034

William F. Gerhold
National Bureau of Standards
Corrosion Section
Washington, DC 20234

Chief of Engineers
U. S. Army
DAEN-MCE-D
Washington, DC 20314

Commander
Naval Ship Systems Command
Code OOC
Washington, DC 20362

Mr. David L. Southey
Code 41A
Bureau of Medicine and Surgery
Navy Department
Washington, DC 20372

U.S. Naval Oceanographic Office
Library - Code 3600
Washington, DC 20373

Director
Naval Research Laboratory
Code 2627
Washington, DC 20375

Public Works Officer
Naval Research Laboratory
4555 Overlook Ave., SW
Washington, DC 20375

Director of Navy Laboratories
Room 300, Crystal Plaza Bldg 5
Department of the Navy
Washington, DC 20376

Commanding Officer
Chesapeake Division - Code 03
Naval Facilities Engineering Command
Washington Navy Yard
Washington, DC 20390

Director, Design Division - 04
Chesapeake Division
Naval Facilities Engineering Command
Washington Navy Yard
Washington, DC 20390

Public Works Officer
Naval Air Facility
Washington, DC 20390

Commandant
Naval District Washington
Public Works Department - Code 412
Washington, DC 20390

Public Works Officer
Naval Security Station
3801 Nebraska Avenue, NW
Washington, DC 20390

Public Works Officer
Naval Communication Station
Washington, DC 20390

Mr. M. R. Whitley
Criteria & Research Branch
Office of Construction Management
General Services Administration
Washington, DC 20405

Commanding Officer
Naval Explosive Ordnance
Disposal Facility - Code TI 1
Indian Head, MD 20640

Public Works Officer
Naval Ordnance Station
Indian Head, MD 20640

Public Works Officer
Naval Air Station
Patuxent River, MD 20670

Commander
Naval Ship Engineering Center
Code 6136
Prince Georges Center
Hyattsville, MD 20782

Commander
Naval Ship Engineering Center
Code 6162
Prince Georges Center
Hyattsville, MD 20782

Technical Library
Naval Ship Engineering Center
622 Center Bldg
Prince Georges Center
Hyattsville, MD 20782

Chief
Marine & Earth Sciences Library
National Oceanic & Atmospheric Admin.
Dept of Commerce
Rockville, MD 20852

M. E. Ringenbach
Engineering Development Lab (C61)
National Oceanic & Atmospheric Admin.
National Ocean Survey
Rockville, MD 20852

Public Works Officer
Naval Ordnance Laboratory, White-Oak
Code 942
Silver Spring, MD 20910

Commanding Officer
ATTN: STEAP-TL
Bldg 305
Aberdeen Proving Ground, MD 21005

Director
Division of Engineering & Weapons
U. S. Naval Academy
Annapolis, MD 21402

Dr. Neil T. Monney
Naval Systems Engineering Dept
U. S. Naval Academy
Annapolis, MD 21402

Public Works Department
U. S. Naval Academy
Annapolis, MD 21402

Library, Code 5642
Annapolis Laboratory
Naval Ship Research & Dev. Center
Annapolis, MD 21402

Public Works Officer
Naval Support Facility
Box 277
Thurmont, MD 21788

U.S. Army Coastal Eng. Research Center
Kingman Building
Fort Belvoir, VA 22060

Public Works Officer
Marine Corps Dev. Education Command
Quantico, VA 22134

Facilities Officer
Office of Naval Research
Code 108
800 North Quincy Street
Arlington, VA 22217

Dr Nicholas Perrone
Code 439
Office of Naval Research
800 North Quincy Street
Arlington, VA 22217

Oceanographer of the Navy
ATTN: Code N712
200 Stovall Street
Alexandria, VA 22332

CAPT Pharo A. Phelps, CEC, USN
Naval Facilities Engineering Command
200 Stovall Street
Alexandria, VA 22332

Commander
Code 0436B
Naval Facilities Engineering Command
200 Stovall Street
Alexandria, VA 22332

Public Works Officer
Naval Weapons Laboratory
Dahlgren, VA 22448

Public Works Officer
Fleet Combat Direction Systems
Training Center, Atlantic
Dam Neck
Virginia Beach, VA 23461

Public Works Officer
Naval Weapons Station
Yorktown, VA 23491

Commanding Officer
Navy Public Works Center
Norfolk, VA 23511

Staff Civil Engineer
Naval Air Station
Norfolk, VA 23511

RDT&E Liaison Officer
Code 09P2
Atlantic Division
Naval Facilities Engineering Command
Norfolk, VA 23511 (2 copies)

Director
Amphibious Warfare Board
Naval Amphibious Base, Little Creek
Norfolk, VA 23521

Public Works Officer
Naval Amphibious Base, Little Creek
Norfolk, VA 23521

General Engineer
Naval Hospital
Portsmouth, VA 23708

Director
Engineering Division - Code 440
Public Works Department
Norfolk Naval Shipyard
Portsmouth, VA 23709

Public Works Officer
Naval Facility, Cape Hatteras
Buxton, NC 27920

Public Works Officer
Marine Corps Air Station
Cherry Point, NC 28533

Public Works Officer
Marine Corps Air Station, New River
Jacksonville, NC 28540

Public Works Officer
Marine Corps Base
Camp Lejuene, NC 28542

Public Works Officer
Charleston Naval Shipyard
Naval Base
Charleston, SC 29408

Staff Civil Engineer
Naval Hospital
Charleston, SC 29408

Public Works Officer
Naval Station
Naval Base
Charleston, SC 29408

RDT&E Liaison Officer
Southern Division - Code 90
Naval Facilities Engineering Command
P. O. Box 10068
Charleston, SC 29411

Staff Civil Engineer
Naval Supply Center
Charleston, SC 29411

Public Works Officer
Naval Hospital
Beaufort, SC 29902

Public Works Officer
Marine Corps Air Station
Beaufort, SC 29902

Public Works Officer
P. O. Box 35
Marine Corps Recruit Depot
Parris Island, SC 29905

Public Works Officer
Naval Air Station, Atlanta
Marietta, GA 30063

Public Works Officer
Navy Supply Corps School
Athens, GA 30601

Public Works Department
Naval Air Station
Glynco, GA 31520

Public Works Officer
Naval Air Station
Albany, GA 31703

Public Works Officer
Marine Corps Supply Center
Albany, GA 31704

Director of Engineering
Naval Air Station
Jacksonville, FL 32212

Public Works Officer
Naval Air Station
Cecil Field, FL 32215

AFCEC/DE
Tyndall Air Force Base, FL 32401

R. E. Elliott
Code 710
Naval Coastal Systems Laboratory
Panama City, FL 32401

Public Works Officer
Naval Coastal Systems Laboratory
Panama City, FL 32401

Staff Civil Engineer
Naval Air Station
Pensacola, FL 32508

Commanding Officer (Code 200)
Navy Public Works Center, Bldg 1
Naval Air Station
Pensacola, FL 32508

Public Works Officer
Naval Air Station, Whiting Field
Milton, FL 32570

Public Works Officer
Naval Training Center
Orlando, FL 32813

Staff Civil Engineer
Naval Training Equipment Center
Orlando, FL 32813

Public Works Officer
Naval Security Group Activity
Homestead, FL 33030

Public Works Officer
Naval Station
Key West, FL 33040

Staff Civil Engineer
Naval Air Station
Key West, FL 33040

Public Works Officer
Naval Air Station, Memphis (84)
Millington, TN 38054

Staff Civil Engineer
Naval Hospital Memphis
Millington, TN 38054

Public Works Officer
Naval Air Station
Meridian, MS 39301

Public Works Officer
Naval Ordnance Station
Louisville, KY 40214

AFIT
Civil Engineering School
Wright-Patterson AFB, OH 45433

Public Works Officer
Naval Avionics Facility
Indianapolis, IN 46218

Public Works Officer
Naval Ammunition Depot
Crane, IN 47522

Public Works Officer
Naval Air Facility, Detroit
Mount Clements, MI 48043

Public Works Officer
Naval Air Station
Glenview, IL 60026

Army Construction Eng. Research Lab.
ATTN: Library
P. O. Box 4005
Champaign, IL 61820

Commanding Officer - Engineering Div.
MRD-Corps of Engineers
Department of the Army
P. O. Box 103, Downtown Station
Omaha, NE 68101

Public Works Department
Maintenance Division
Naval Air Station, New Orleans
Belle Chasse, LA 70037

Public Works Officer
Naval Air Station, New Orleans
Belle Chasse, LA 70037

Public Works Officer
Naval Ammunition Depot
McAlester, OK 74501

Public Works Officer
Naval Air Station
Dallas, TX 75211

Public Works Officer
Naval Air Station
Chase Field
Beeville, TX 78102

Public Works Officer
Naval Air Station
Corpus Christi, TX 78419

Public Works Department
Marine Corps Air Station
Yuma, AZ 85364

Technical Reference Division
Headquarters, Fort Huachuca
Fort Huachuca, AZ 85613

AFWL
CE Division
Kirtland AFB, NM 87117

Public Works Officer
Naval Ordnance Missile Test Facility
White Sands Missile Range, NM 88002

Public Works Officer
Naval Air Station
Fallon, NV 89406

Public Works Officer
Naval Ammunition Depot
Hawthorne, NV 89415

Public Works Officer
Naval Air Station
Los Alamitos, CA 90720

Public Works Officer
Naval Weapons Station
Seal Beach, CA 90740

Public Works Officer
Naval Station
Long Beach, CA 90801

Dr Arthur R. Laufer
Office of Naval Research, BROFF
1030 East Green Street
Pasadena, CA 91106

Officer in Charge
Pasadena Laboratory - Naval Undersea Center
ATTN: Technical Library
3202 E. Foothill Blvd
Pasadena, CA 91107

Asst. Public Works Officer
Naval Weapons Station
Fallbrook Annex
Fallbrook, CA 92028

Staff Civil Engineer
Naval Air Station
Imperial Beach, CA 92032

Public Works Officer
Marine Corps Base
Camp Pendleton, CA 92055

Dr J. D. Stachiw
Code 6505
Naval Undersea Center
San Diego, CA 92132

Mr. R. E. Jones
Code 65402
Naval Undersea Center
San Diego, CA 92132

Technical Library
Code 1311
Naval Undersea Center
San Diego, CA 92132

Public Works Officer
Code 75
Naval Undersea Center
San Diego, CA 92132

Staff Civil Engineer
Naval Training Center
San Diego, CA 92133

Public Works Officer
Naval Administrative Command
Naval Training Center
San Diego, CA 92133

Civil Staff Engineer
Naval Hospital
San Diego, CA 92134

Public Works Officer
Naval Air Station
North Island
San Diego, CA 92135

Staff Civil Engineer
Naval Station
San Diego, CA 92136

Commanding Officer
Navy Public Works Center
Naval Base
San Diego, CA 92136

Public Works Officer
Naval Air Station
Miramar
San Diego, CA 92145

Public Works Officer
Naval Amphibious Base
Coronado
San Diego, CA 92155

Public Works Officer
Naval Air Facility
El Centro, CA 92243

Public Works Officer
Marine Corps Base
Bldg 1130
Twentynine Palms, CA 92278

Public Works Officer
Marine Corps Supply Center
Barstow, CA 92311

Public Works Department (151)
Marine Corps Air Station
El Toro
Santa Ana, CA 92709

Commanding Officer
Naval Missile Center
Code 5632.2, Technical Library
Point Mugu, CA 93042

Office of Patent Counsel
Code PC (Box 40)
Naval Missile Center
Point Mugu, CA 93042

Public Works Officer
Naval Air Station
Point Mugu, CA 93042

Public Works Officer
Code 82
Naval Construction Battalion Center
Port Hueneme, CA 93043

Librarian, Code 9215
Construction Equipment Department
Naval Construction Battalion Center
Port Hueneme, CA 93043

Commander
31st Naval Construction Regiment
Naval Construction Battalion Center
Port Hueneme, CA 93043

Commanding Officer
Code 155
Naval Construction Battalion Center
Port Hueneme, CA 93043

Commanding Officer
Naval Schools of Construction
Port Hueneme, CA 93043

Public Works Officer (70)
Naval Weapons Center
China Lake, CA 93555

Public Works Officer
Naval Facility, Big Sur
Big Sur, CA 93920

Superintendent
Attn: Library (Code 2124)
Naval Postgraduate School
Monterey, CA 93940

Public Works Officer
Public Works Dept
Naval Postgraduate School
Monterey, CA 93940

Dr. Edward B. Thornton
Department of Oceanography
Naval Postgraduate School
Monterey, CA 93940

Public Works Officer
Naval Air Station
Moffett Field, CA 94035

Commanding Officer
Western Division - Code 09PA
Naval Facilities Engineering Command
P. O. Box 727
San Bruno, CA 94066

Commanding Officer
Western Division - Code 04
Naval Facilities Engineering Command
P. O. Box 727
San Bruno, CA 94066

Commanding Officer
Western Division - Code 04B
Naval Facilities Engineering Command
P. O. Box 727
San Bruno, CA 94066

Commanding Officer
Western Division - Code 05
Naval Facilities Engineering Command
P. O. Box 727
San Bruno, CA 94066

Commanding Officer
Western Division - Code 112
Naval Facilities Engineering Command
P. O. Box 727
San Bruno, CA 94066

Public Works Officer
Naval Station
Treasure Island
San Francisco, CA 94130

Asst. Resident OIC of Construction
Bldg 506
Hunters Point Naval Shipyard
San Francisco, CA 94135

Public Works Officer
San Francisco Bay Naval Shipyard
Hunters Point Division
San Francisco, CA 94135

Public Works Department (183)
Naval Air Station
Alameda, CA 94501

Public Works Officer
Mare Island Naval Shipyard
Vallejo, CA 94592

Asst. Public Works Officer
Naval Support Activity
Mare Island Naval Shipyard
Vallejo, CA 94592

Public Works Officer
Code 70
Naval Supply Center
Oakland, CA 94625

Public Works Officer
Naval Hospital
Oakland, CA 94627

Mr. H. Wheeler
Code 73.13
Naval Fuel Department
Point Molate
Richmond, CA 94804

Public Works Officer
Naval Communication Station San Francisco
Rough and Ready Island
Stockton, CA 95203

Public Works Officer
Naval Facility, Centerville Beach
Ferndale, CA 95536

Base Civil Engineer
Det 3, 15th ABW (PACAF)
APO San Francisco 96305

Director, Engineering Division
Officer in Charge of Construction
Naval Facilities Engineering Command
Contracts, Southwest Pacific
APO San Francisco 96528

Headquarters
Kwajalein Missile Range
Box 26, Attn: SSCR-RKL-C
APO San Francisco 96555

Commanding Officer
Mobile Construction FOUR
FPO San Francisco 96601

Commanding Officer
Mobile Construction Battalion TEN
FPO San Francisco 96601

Staff Civil Engineer
Pearl Harbor Naval Shipyard
Box 400
FPO San Francisco 96610

Staff Civil Engineer
Naval Supply Center
Box 300
FPO San Francisco 96610

Commander Pacific Division
Naval Facilities Engineering Command
FPO San Francisco 96610

RDT&E Liaison Officer
Pacific Division - Code 403
Naval Facilities Engineering Command
FPO San Francisco 96610

Mr. T. M. Ishibashi
Navy Public Works Center
Engineering Department - Code 200
FPO San Francisco 96610

Staff Civil Engineer
Naval Supply Center
Box 300
FPO San Francisco 96610

Public Works Officer
U.S. Naval Air Station
FPO San Francisco 96611

Public Works Officer
Engineering Division
Naval Ammunition Depot
FPO San Francisco 96612

Public Works Officer
U. S. Naval Station
Box 15
FPO San Francisco 96614

Mr. D. K. Moore
Hawaii Laboratory
Naval Undersea Center
FPO San Francisco 96615

Public Works Officer
U.S. Marine Corps Air Station
FPO San Francisco 96615

Staff Civil Engineer
U. S. Naval Communication Station
FPO San Francisco 96630

Staff Civil Engineer
U.S. Naval Station
FPO San Francisco 96630

Officer in Charge of Construction
Naval Facilities Engineering Command
Contracts, Marianas
FPO San Francisco 96630

Staff Civil Engineer
U.S. Naval Station
FPO San Francisco 96630

Technical Library
Engineering Department
U. S. Navy Public Works Center
Box 6
FPO San Francisco 96651

Staff Civil Engineer
U.S. Naval Station
FPO San Francisco 96651

Staff Civil Engineer
U.S. Naval Station
FPO San Francisco 96654

Asst. Public Works Officer
San Migual, Naval Communications Station
Box 1585
FPO San Francisco 96656

Public Works Officer
U.S. Naval Communication Station
FPO San Francisco 96680

Officer in Charge of Construction
Naval Facilities Engineering Command
Contracts
FPO San Francisco 96680

U.S. Naval Support Force Antarctica
Detachment 1
FPO San Francisco 96690

Public Works Officer
Naval Facility
Coos Head Empire Station
Coos Bay, OR 97420

Public Works Officer
Naval Support Activity
Seattle, WA 98115

Public Works Officer
Naval Air Station
Whiley Island
Oak Harbor, WA 98277

Public Works Dept., Code 400
Puget Sound Naval Shipyard
Bremerton, WA 98314

Public Works Officer
Naval Torpedo Station
Keyport, WA 98345

Commanding Officer
U.S. Navy Public Works Center
Box 13
FPO Seattle 98762

Commanding Officer
U. S. Naval Air Facility
Box 15
FPO Seattle 98767

Public Works Officer
U.S. Naval Security Group Activity
FPO Seattle 98768

Public Works Officer
Fleet Activities
FPO Seattle 98770

Public Works Officer
Marine Corps Air Station (H)
FPO Seattle 98772

Public Works Officer
Marine Corps Base
Camp Smedley D. Butler
FPO Seattle 98773

Public Works Officer
U. S. Naval Station
FPO Seattle 98791

Public Works Officer
U.S. Naval Communication Station
Box 30
FPO Seattle 98791

Colleges, etc.

Prof. W. E. Heronemus
Civil Engineering Dept.
University of Massachusetts
Amherst, MA 01002

MIT Libraries
Technical Reports - Room 14 E-210
Massachusetts Institute of Technology
Cambridge, MA 02139

Document Library L0-206
Woods Hole Oceanographic Institution
Woods Hole, MA 02543

Prof. R. W. Corell
Mechanical Engineering Dept.
Kingsbury Hall
University of New Hampshire
Durham NH 03824

Reprint Custodian
Dept. of Nautical Science
U. S. Merchant Marine Academy
Kings Point, NY 11024

Mr. R. F. Snyder
Ordnance Research Laboratory
Pennsylvania State University
State College, PA 16801

Professor Adrian F. Richards
Marine Geotechnical Laboratory
Lehigh University
Bethlehem, PA 18015

Dr. Houan Yeh
Towne School of Civil & Mechanical Eng.
University of Pennsylvania
Philadelphia, PA 19104

Mr. T. W. Mermel
4540 43rd St., NW
Washington, D.C. 20016

Library of Congress
Science & Technology Division
Washington, DC 20540

W. F. Searle, Jr.
National Academy of Engineering
808 Timber Branch Parkway
Alexandria, VA 22302

Public Documents Department
Wm. R. Perkins Library
Duke University
Durham, NC 27706

Dr R. C. Jordan
Dept of Mechanical Engineering
University of Minnesota
Minneapolis, MN 55455

Dr N. M. Newmark
1114 Civil Engineering Bldg
University of Illinois
Urbana, IL 61801

Professor W. J. Hall
1108 Civil Engineering Bldg
University of Illinois
Urbana, IL 61801

Metz Reference Room
Civil Engineering Dept
B106 Civil Engineering Bldg
University of Illinois
Urbana, IL 61801

Mr. G. A. Sutton
Planning & Development
State Highway Commission
State Office Bldg
Topeka, KS 66612

Acquisition Dept - Serials Section
University of Nebraska Libraries
Lincoln, NE 68508

Robert D. Tent
Undersea Services Division
Fluor Ocean Services Inc
P. O. Drawer 310
Houma, LA 70360

Department of Oceanography
Texas A & M University
College Station, TX 77843

Civil Engineering Dept
Texas A & M University
College Station, TX 77843

R. C. Dehart
Southwest Research Institute
8500 Culebra Road
San Antonio, TX 78228

Wang Civil Engineering Research Facility
P. O. Box 188 - CERF
University Station
University of New Mexico
Albuquerque, NM 87106

Aerospace Corporation
Acquisitions Group
P. O. Box 92957
Los Angeles, CA 90009

TRW Systems
Attn: P. K. Dai R1/2178
1 Space Park
Redondo Beach, CA 90278

Dr F. N. Spiess
Marine Physical Laboratory
Of the Scripps Institution of Oceanography
University of California
San Diego, CA 92152

Engineering Library
Stanford University Libraries
Stanford, CA 94305

Dept of Naval Architecture
College of Engineering
University of California
Berkeley, CA 94720

Engineering Library
University of California
Berkeley, CA 94720

Melvin R. Ramey
Civil Engineering Dept
University of California, Davis
Davis, CA 95616

H. Norby Neilsen
University of Hawaii
Honolulu, HI 96822

Dr. Woods
Office of Naval Research
Branch Office
495 Summer Street
Boston, MA 02210

Dr. Rockwell
Lehigh University
Bethelem, PA 18015

Dr. J. A. Owczarek
Lehigh University
Bethelem, PA 18015

UNCLASSIFIED
Security Classification

DOCUMENT CONTROL DATA - R & D

(Security classification of title, body of abstract and indexing annotation must be entered when the overall report is classified)

1. ORIGINATING ACTIVITY (Corporate author) Naval Civil Engineering Laboratory Port Hueneme, California 93043	2a. REPORT SECURITY CLASSIFICATION Unclassified 2b. GROUP

3. REPORT TITLE

A FLUIDIC SYSTEM FOR MIXING TWO FLUIDS – FINAL STUDY

4. DESCRIPTIVE NOTES *(Type of report and inclusive dates)*

5. AUTHOR(S) *(First name, middle initial, last name)*

D. Pal

6. REPORT DATE December 1973	7a. TOTAL NO. OF PAGES 74	7b. NO. OF REFS 8

8a. CONTRACT OR GRANT NO.	9a. ORIGINATOR'S REPORT NUMBER(S) TN-1314
b. PROJECT NO. ZFXX-512-001-005	
c.	9b. OTHER REPORT NO(S) (Any other numbers that may be assigned this report)
d.	

10. DISTRIBUTION STATEMENT

Approved for public release; distribution unlimited.

11. SUPPLEMENTARY NOTES	12. SPONSORING MILITARY ACTIVITY Director of Navy Laboratories Washington, D.C. 20376

13. ABSTRACT

The development of a double leg elbow proportional fluid amplifier to handle 5.85 gpm of water flow rate is described in detail. The amplifier has linear output flow characteristics with a gain of 50 and can switch flow from one output to the other completely. Based upon the experimental results, analytical expressions are developed which clearly show the effects of the active and passive legs flow parameters, the control flow, and the size and location of the output ports on amplifier's performance and they can be used in designing an amplifier of a desired flow capacity. Analytical expressions to predict the performance of the amplifier are also given. A mixing element comprised of two double leg elbow amplifiers stacked together to mix two fluids was designed and tested successfully.

DD FORM 1 NOV 65 1473 (PAGE 1)

S/N 0101-807-6801

UNCLASSIFIED
Security Classification

14 KEY WORDS	LINK A		LINK B		LINK C	
	ROLE	WT	ROLE	WT	ROLE	WT
Fluid amplifier						
double leg elbow						
Fluid mixer						
Mixture ratio						
Variable fluid resistor						